



HAL
open science

Bioen-OSMOSE: A bioenergetic marine ecosystem model with physiological response to temperature and oxygen

Alaia Morell, Yunne-jai Shin, Nicolas Barrier, Morgane Travers-Trolet, Ghassen Halouani, Bruno Ernande

► To cite this version:

Alaia Morell, Yunne-jai Shin, Nicolas Barrier, Morgane Travers-Trolet, Ghassen Halouani, et al.. Bioen-OSMOSE: A bioenergetic marine ecosystem model with physiological response to temperature and oxygen. *Progress in Oceanography*, 2023, 216, 103064 (16p.). 10.1016/j.pocean.2023.103064 . hal-04204090

HAL Id: hal-04204090

<https://hal.science/hal-04204090>

Submitted on 23 Feb 2024

HAL is a multi-disciplinary open access archive for the deposit and dissemination of scientific research documents, whether they are published or not. The documents may come from teaching and research institutions in France or abroad, or from public or private research centers.

L'archive ouverte pluridisciplinaire **HAL**, est destinée au dépôt et à la diffusion de documents scientifiques de niveau recherche, publiés ou non, émanant des établissements d'enseignement et de recherche français ou étrangers, des laboratoires publics ou privés.



Distributed under a Creative Commons Attribution - NonCommercial - NoDerivatives 4.0 International License

1 Bioen-OSMOSE: A bioenergetic marine ecosystem 2 model with physiological response to temperature 3 and oxygen

4 *Alaia Morell^{1,2}, Yunne-Jai Shin², Nicolas Barrier², Morgane Travers-Trolet³, Ghassen Halouani¹,*
5 *Bruno Ernande^{2,4}*

6 **Author details**

7 1 IFREMER, Unité halieutique Manche Mer du Nord Ifremer, HMMN, Boulogne sur mer, France,
8 alaia.morell@gmail.com

9 2 MARBEC, Univ. Montpellier, Ifremer, CNRS, IRD, Sète/Montpellier, France.

10 3 DECOD (Ecosystem Dynamics and Sustainability), IFREMER, INRAE, Institut Agro, 44311
11 Nantes, France

12 4 International Institute for Applied Systems Analysis (IIASA), A-2361 Laxenburg, Austria.

13 **ABSTRACT**

14 1 - Marine ecosystem models have been used to project the impacts of climate-induced changes in
15 temperature and oxygen on biodiversity mainly through changes in species spatial distributions and
16 primary production. However, fish populations may also respond to climatic pressures via
17 physiological changes, leading to modifications in their life history that could either mitigate or
18 worsen the consequences of climate change.

19 2- Building on the individual-based multispecies ecosystem model OSMOSE, Bioen-OSMOSE has been
20 developed to account for high trophic levels' physiological responses to temperature and oxygen in
21 future climate projections. This paper presents an overview of the Bioen-OSMOSE model, mainly
22 detailing the new developments. These consist in the implementation of a bioenergetic sub-model
23 that mechanistically describes somatic growth, sexual maturation and reproduction as they emerge
24 from the energy fluxes sustained by food intake under the hypotheses of a biphasic growth model
25 and plastic maturation age and size represented by a maturation reaction norm. These fluxes depend
26 on temperature and oxygen concentration, thus allowing plastic physiological responses to climate
27 change.

28 3 - To illustrate the capabilities of Bioen-OSMOSE to represent realistic ecosystem dynamics, the
29 model is applied to the North Sea ecosystem. The model outputs are confronted with population
30 biomass, catch, maturity ogive, mean size-at-age and diet data of each species of the fish community.
31 A first exploration of current species spatial variability in response to temperature or oxygen is
32 presented in this paper. The model succeeds in reproducing observations, with good performances
33 for all indicators.

34 4 - This new model development opens the scope for new fields of research such as the exploration
35 of seasonal or spatial variation in life history in response to biotic and abiotic factors at the individual,
36 population and community levels. Understanding such variability is crucial to improve our knowledge
37 on potential climate change impacts on marine ecosystems and to make more reliable projections
38 under climate change scenarios.

39 **Keyword**

40 Bioenergetic, Food web, Hypoxia, Marine ecosystem model, Phenotypic plasticity, Thermal tolerance

41 **1. Introduction**

42 The development of increasingly realistic marine ecosystem models (MEMs) is needed to improve
43 understanding and knowledge about marine ecosystems, which is one of the main challenges of the
44 UN Decade of the Oceans (Heymans et al., 2020). MEMs are end-to-end models representing
45 ecosystems from primary production to top predators, linking the species and/or functional groups
46 via trophic interactions. These models also account for abiotic and human activity impacts on
47 ecosystem dynamics (Rose et al., 2010; Steenbeek et al., 2021; Travers et al., 2007). MEMs are still
48 being improved through the development of sub-models that increase their reliability in supporting
49 ecosystem-based management (Pikitch et al., 2004; Rose et al., 2010).

50 The rates of ocean temperature rise and deoxygenation make urgent the development of
51 mechanistic tools to forecast realistically their impacts from the physiology of marine organisms, to
52 the population demographic impacts and to the consequence on marine trophic webs (Breitburg et
53 al., 2018; Urban et al., 2016). Efforts to model the temperature impacts on marine biodiversity at the
54 ecosystem level has so far focused mainly on the bottom-up effect of temperature on the ecosystem
55 via changes in primary production (Lefort et al., 2015; Moullec et al., 2019) and on the distribution
56 shift of species according to their preferred temperature (Albouy et al., 2014; Fernandes et al., 2013;
57 Moullec et al., 2019; Serpetti et al., 2017). Mechanistic physiological response to temperature in
58 MEM is modeled in size spectrum models and to our knowledge is not currently incorporated into an
59 explicit multispecies model (Lefort et al., 2015; Maury, 2010). Although oxygen concentration is

60 considered as a main pressure on marine biodiversity (Laffoley & Baxter, 2019), the oxygen
61 physiological impact on marine ecosystems is still not explicitly modeled in MEMs.

62 The core of recent model developments linking environmental conditions and physiological response
63 is primarily on single-species models. These frameworks mechanistically describe life history cycles
64 and metabolic fluxes. The response of metabolic rates to temperature is used in several frameworks
65 (Gillooly et al., 2002; Kooijman, 2010) which are applied to project future population dynamics and
66 spatial distribution under climate change scenarios. The response of metabolic rates to oxygen
67 through its impact on ingestion (Thomas et al., 2019) has been recently introduced in the Dynamic
68 Energy Budget framework to study the impact of hypoxia on population dynamics (Lavaud et al.,
69 2019).

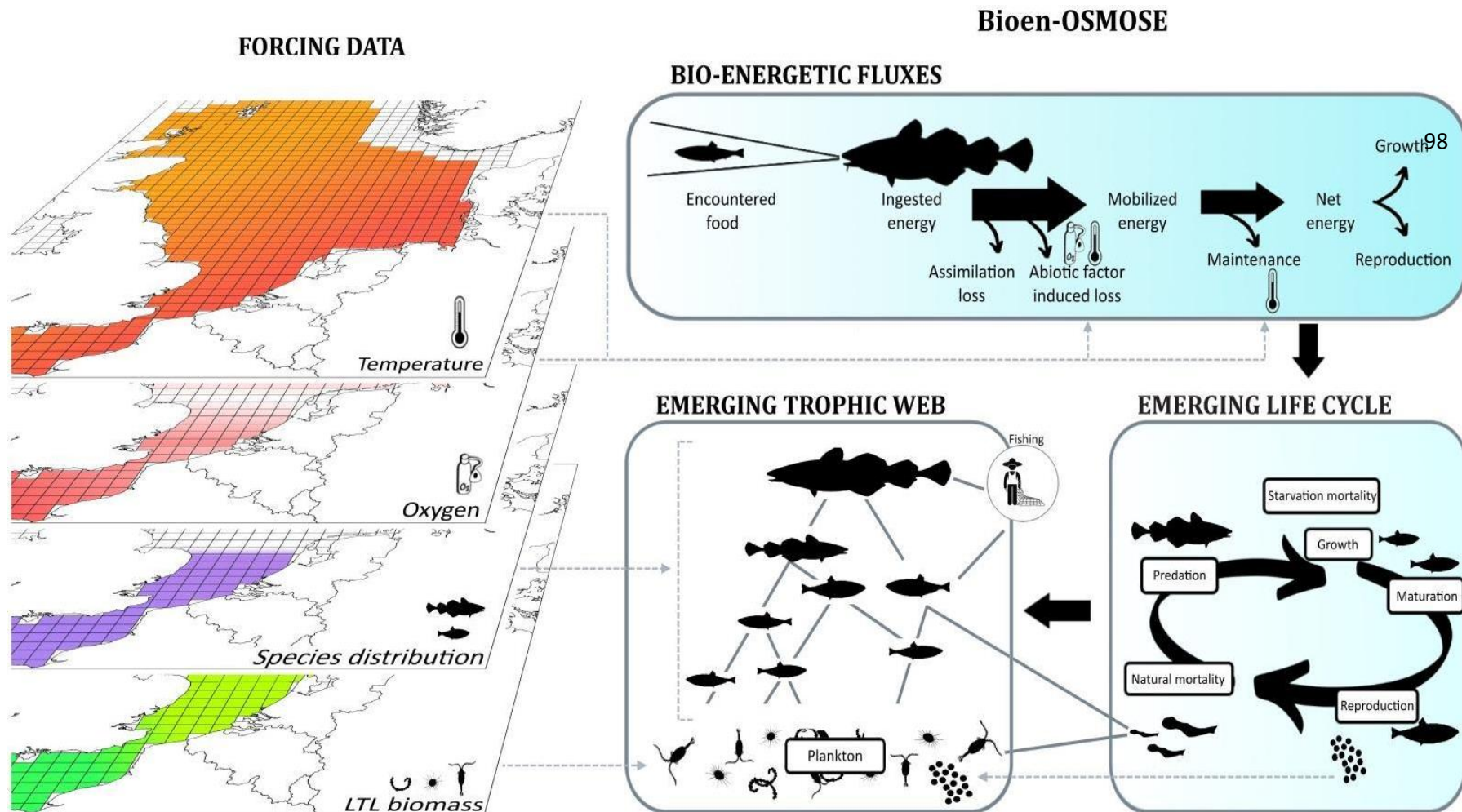
70 The model Bioen-OSMOSE is a new framework that mechanistically describes the emergence of life
71 history traits through an explicit description of the underlying bioenergetic fluxes and their response
72 to food, temperature and oxygen variation in a multispecies food web model. It has been developed
73 from the OSMOSE framework (Shin & Cury, 2004; www.osmose-model.org), which is an individual-
74 based, spatially and temporally explicit, multispecies model for regional marine ecosystems.
75 Designed to be possibly coupled to ocean and biogeochemical models, it includes the components of
76 the entire ecosystem, from primary production to fish populations and human fishing activity, but
77 the core of the model describes the dynamics of fish and macroinvertebrate species. In this paper,
78 we provide a detailed description of the principles and equations of the Bioen-OSMOSE framework,
79 as well as parameterization guidelines (detailed in Supporting Information). An application to the
80 North Sea ecosystem is provided as a case study example. We then confront simulation outputs from
81 the North Sea example to observed data to assess the consistency of the new model development
82 and explore spatial variability in fish metabolic fluxes in response to temperature and oxygen.

83 **2. Method**

84 **2.1. Model description**

85 The Bioen-OSMOSE model (Fig. 1) represents fish individual physiological responses to temperature
86 and oxygen variations and their consequences on fish communities in marine ecosystems. It is an
87 individual-based, spatially and temporally explicit multispecies model accounting for trophic
88 interactions. The main characteristics of the model are opportunistic predation based on size
89 adequacy and spatiotemporal co-occurrence of predators and prey, the mechanistic description of
90 individuals' life-history traits emerging from bioenergetics. The aims of the model are to explore the
91 functioning of marine trophic webs, the ecosystem impacts of individual physiological modifications

92 due to temperature and oxygen, and the consequences of fishing pressure or climate change, from
93 individual phenotype, to the population and to the community scale. The Bioen-OSMOSE model
94 extends the existing OSMOSE model by (i) explicitly accounting for the mechanistic dependence of
95 life-history traits on bioenergetics and (ii) describing intra- and inter-specific phenotypic variability
96 originating from plastic responses to spatio-temporal biotic and abiotic factor variations. A process
97 overview is given in Supporting Information S1.



99 Figure 1: Graphical description of the Bioen-OSMOSE model. In the Bioen-OSMOSE model trophic relationships emerge from spatio-temporal co-occurrence
 100 and size adequacy between predators and prey, the former resulting from ontogenic spatial distributions and possibly LTL biomass distribution. The life
 101 cycle emerges from the underlying bioenergetic fluxes that describe the internal processes from energy ingestion (which relies on the encountered prey) to
 102 growth, maturation and reproduction. The internal fluxes are partly driven by environmental conditions, i.e, temperature and oxygen.

103 2.1.1. Biological unit, state variables and spatial characteristics

104 The biological unit of the model is a school (a super-individual in individual-based modeling
105 terminology). It is formed by individuals from the same species that are biologically identical. The
106 state variables characterizing a school i at time step t belong to four categories (see Table 1 for state
107 variable definitions and their units):

- 108 - Ontogenic state of individuals described by their age $a(i, t)$, somatic mass $w(i, t)$ and
109 gonadic mass $g(i, t)$;
- 110 - Abundance, namely the number of individuals in the school $N(i, t)$;
- 111 - Spatial location, i.e., the grid cell $c(i, t)$ where the school is located; and
- 112 - Taxonomic identity, i.e., the species $s(i)$ to which the school belongs.

113 Fish schools are distributed on a horizontal spatial grid that is composed of regular cells and that
114 covers the geographical range of the ecosystem represented. A cell c is characterized by its spatial
115 coordinates, longitude $x(c)$ and latitude $y(c)$, and several other variables: (i) the vertically-
116 distributed values (z vertical layers) of k physico-chemical factors $pc_k(c, t, z)$ (such as temperature
117 $T(c, t, z)$ or the level of oxygen saturation (%) $[O_2](c, t, z)$) and (ii) the biomass of all low trophic
118 level (LTL) groups (indexed by j) $B_{LTL}(c, j, t)$ that are not explicitly modeled in Bioen-OSMOSE but
119 provided as input from coupled hydrodynamic and biogeochemical models.

120 Below we describe the bioenergetic sub-model that we developed to describe individual life-history
121 and its responses to environmental variations. The individuals described with this level of detail
122 belong to high trophic level (HTL) species, mainly fish and macroinvertebrate species.

123 2.1.2. Individual life history description

124 Individual life history emerges from underlying bioenergetic fluxes which are described according to
125 a biphasic growth model (Fig. 1) (Andersen, 2019; Boukal et al., 2014; Quince et al., 2008). The body
126 mass-dependent energy fluxes are allocated according to physiological tradeoffs between competing
127 processes: maintenance, somatic growth and gonadic growth. The sexual maturation of individuals
128 relies on the concept of maturation reaction norms that depicts how the process of maturation
129 responds plastically to variation in body growth (Heino et al., 2002; Stearns & Koella, 1986). This
130 combination of processes mechanistically describes how somatic growth, sexual maturation and
131 reproduction emerge from energy fluxes sustained by food intake resulting from opportunistic size-
132 based predator-prey interactions.

133 On top of the biphasic growth model, individuals' energy mobilization and maintenance energetic
134 costs depend on dissolved oxygen concentration and temperature so that the resulting metabolic
135 rate (the net energy available for new tissue production) and thus somatic and gonadic growth vary
136 with these abiotic parameters in a way that conforms to the oxygen- and capacity-limited thermal
137 tolerance theory (OCLTT; Pörtner, 2001) and more generally to thermal performance curves (TPC;
138 Angilletta, 2009).

139 In the following description, energetic fluxes are expressed in somatic mass unit equivalents under
140 the assumption that the ratio of energy density between somatic and gonadic tissues η is
141 independent of size. All the parameters of the bioenergetic and life-history sub-model are species-
142 specific parameters except one parameter is constant across species, namely the Boltzmann constant
143 (Table 2).

144 2.1.3. Ingestion, assimilation and mobilization

145 For an individual in school i , the ingested food $I(i, t)$ at time step t is described by a Holling's type 1
146 functional response (Holling, 1959) that depends on its somatic mass $w(i, t)$ (Christensen & Walters,
147 2004; Holt & Jorgensen, 2014; Shin & Cury, 2004) in two ways. First, it determines the prey biomass
148 $P(i, t)$ available to an individual of school i . All other fish schools and LTL organisms (from the forcing
149 biogeochemical model) that are present in the same grid cell $c(i, t)$ are potential prey if their body
150 size is compatible with a minimum R_{min} (Shin & Cury, 2004) and a maximum R_{max} predator to prey
151 size ratio based on individual total length $L(i, t) = \left(\frac{w(i, t)}{k}\right)^{\frac{1}{\alpha}}$ (Travers et al., 2009) so that:

$$P(i, t) = \frac{\sum_j \gamma(i, j) B(j, t)}{N(i, t)}$$

152 with $j \in \left\{j \mid (c(j, t) = c(i, t)) \cap \left(\frac{L(i, t)}{R_{max}} \leq L(j, t) \leq \frac{L(i, t)}{R_{min}}\right)\right\}$ (1)

153 where k and α are the allometric length-somatic mass relationship coefficient and exponent,
154 respectively, $\gamma(i, j)$ is the accessibility coefficient of potential prey school j to school i that is
155 essentially determined by the position in the water column of species $s(j)$ relative to species $s(i)$
156 according to their life stage, and $B(j, t) = N(j, t) w(j, t)$ is the biomass of prey school j at time step
157 t . The maximum possible food ingestion rate scales with the mass with a scaling exponent β . The
158 ingested food can then be written as:

159 $I(i, t) = f(P(i, t)) = \min(P(i, t); I_{max} \psi(i, t) w(i, t)^\beta)$ (2)

160 with I_{max} the maximum ingestion rate per mass unit at exponent β (or mass-specific maximum
161 ingestion rate) of individuals in school i and $\psi(i, t)$ a multiplicative factor that depends on their life
162 stage such that:

$$163 \quad \psi(i, t) = \begin{cases} \theta & \text{if } a(i, t) < a_l \\ 1 & \text{otherwise} \end{cases} \quad (3)$$

164 where a_l is the age at the end of an early-life fast-growth period (e.g., larval period or the larval and
165 post-larval period, defined according to data availability, see Supporting Information S2) and θ a
166 multiplicative factor accounting for higher mass-specific ingestion rate at this stage. A portion ξ of
167 the ingested food $I(i, t)$ is assimilated, $(1 - \xi)$ being lost due to excretion and feces egestion.

168 Reserves are not modeled in Bioen-OSMOSE: the assimilated energy is directly mobilized. The
169 difference between assimilated and mobilized energy depends on oxygen and temperature
170 conditions (Fig. 2). Mobilized energy E_M , referred to as active metabolic rate in the ecophysiology
171 literature, fuels all metabolic processes such as maintenance, digestion, foraging, somatic growth,
172 gonadic growth, etc... The mobilization of energy relies on the use of oxygen to transform the energy
173 held in the chemical bonds of nutrients into a usable form, namely ATP (Clarke, 2019). In
174 consequence, the maximum possible energy mobilized depends (i) directly on dissolved oxygen
175 saturation that sets up an upper limit to mobilization at a given temperature and (ii) as temperature
176 increases, on the capacity of individuals to sustain oxygen uptake and delivery for ATP production.
177 The mobilized energy rate E_M is thus described by:

$$178 \quad E_M(i, t) = \xi I(i, t) \lambda([O_2](i, t)) \varphi_M(T(i, t)) \quad (4)$$

179 with $\lambda([O_2](i, t))$ and $\varphi_M(T(i, t))$ being the mobilization responses to dissolved oxygen saturation
180 $[O_2](i, t) = [O_2](c(i, t))$ and temperature $T(i, t) = T(c(i, t))$, respectively, encountered by school i
181 in the grid cell $c(i, t)$. These are scaled between 0 and 1 such that, in optimal oxygen saturation and
182 temperature conditions, all assimilated energy $E_M(i, t) = \xi I(i, t)$ can be mobilized and, in
183 suboptimal conditions, only a fraction of assimilated energy can be mobilized $E_M(i, t) < \xi I(i, t)$.

184 More precisely, the effect of dissolved oxygen is described by a dose-response function $\lambda(\cdot)$ (Thomas
185 et al., 2019) which increases with the saturation of dissolved oxygen:

$$186 \quad \lambda([O_2]) = c_{0,1} \frac{[O_2]}{[O_2] + c_{0,2}} \quad (5)$$

187 with parameters $c_{O,1}$ and $c_{O,2}$ the asymptote and the slope of the dose-response function. The effect
 188 of temperature $\varphi_M(\cdot)$ is such that first, energy mobilization increases with temperature according to
 189 an Arrhenius-like law due to chemical reaction rate acceleration until reaching limitation in
 190 individuals' ventilation and circulation capacity. Hence, oxygen uptake and delivery for energy
 191 mobilization saturates or even decreases at high temperatures, potentially due to temperature
 192 dependence of the rate of enzyme-catalyzed chemical reactions (Arcus et al., 2016) or enzyme
 193 denaturation (Pawar et al., 2015). This effect is described according to the Johnson & Lewin (1946)
 194 model (Pawar et al., 2015):

$$195 \quad \varphi_M(T) = \Phi \frac{e^{-\frac{\varepsilon_M}{k_B T}}}{1 + \frac{\varepsilon_M}{\varepsilon_D - \varepsilon_M} e^{\frac{\varepsilon_D}{k_B} \left(\frac{1}{T_p} - \frac{1}{T}\right)}} \quad (6)$$

196 with k_B the Boltzmann constant, ε_M the activation energy for the Arrhenius-like increase in mobilized
 197 energy with temperature T before reaching its peak value at T_p , ε_D the activation energy when the
 198 energy mobilization declines with T above T_p , and $\Phi = \left(1 + \frac{\varepsilon_M}{\varepsilon_D - \varepsilon_M}\right) e^{\frac{\varepsilon_M}{k_B T_p}}$ a standardizing constant
 199 ensuring that $\varphi_M(T_p) = 1$.

200 2.1.4. Maintenance

201 The mobilized energy E_M fuels all metabolic processes starting in priority with the costs of
 202 maintenance of existing tissues E_m which is often referred to as the standard metabolic rate in the
 203 ecophysiology literature. Here, we also include in the maintenance costs, the routine activities of
 204 individuals, including foraging and digestion, so that they are actually best compared to the routine
 205 metabolic rate in the ecophysiology literature. The maintenance costs are explicitly modeled to
 206 describe the share of mobilized energy between maintenance and the production of new tissues
 207 (Charnov et al., 2001; Holt & Jorgensen, 2014), with precedence of the former over the latter, as well
 208 as to link mechanistically starvation mortality to energetic starvation when neither mobilized energy
 209 nor gonad energy reserves can cover the costs of maintenance (see next section on new tissue
 210 production for more details). The maintenance energy rate E_m scales with the individual's somatic
 211 mass $w(i, t)$ with the same exponent β as the maximum ingestion rate. The maintenance rate also
 212 increases with the temperature $T(i, t)$ experienced by individuals according to the Arrhenius law
 213 (Brown et al., 2004; Gillooly et al., 2002; Kooijman, 2010) and can be described as:

$$214 \quad E_m(i, t) = c_m w(i, t)^\beta \varphi_m(T(i, t)) \quad (7)$$

215 with C_m the mass-specific maintenance rate and $\varphi_m(\cdot)$ the Arrhenius function m defined as:

$$216 \quad \varphi_m(T) = e^{-\frac{\varepsilon_m}{k_B T}} \quad (8)$$

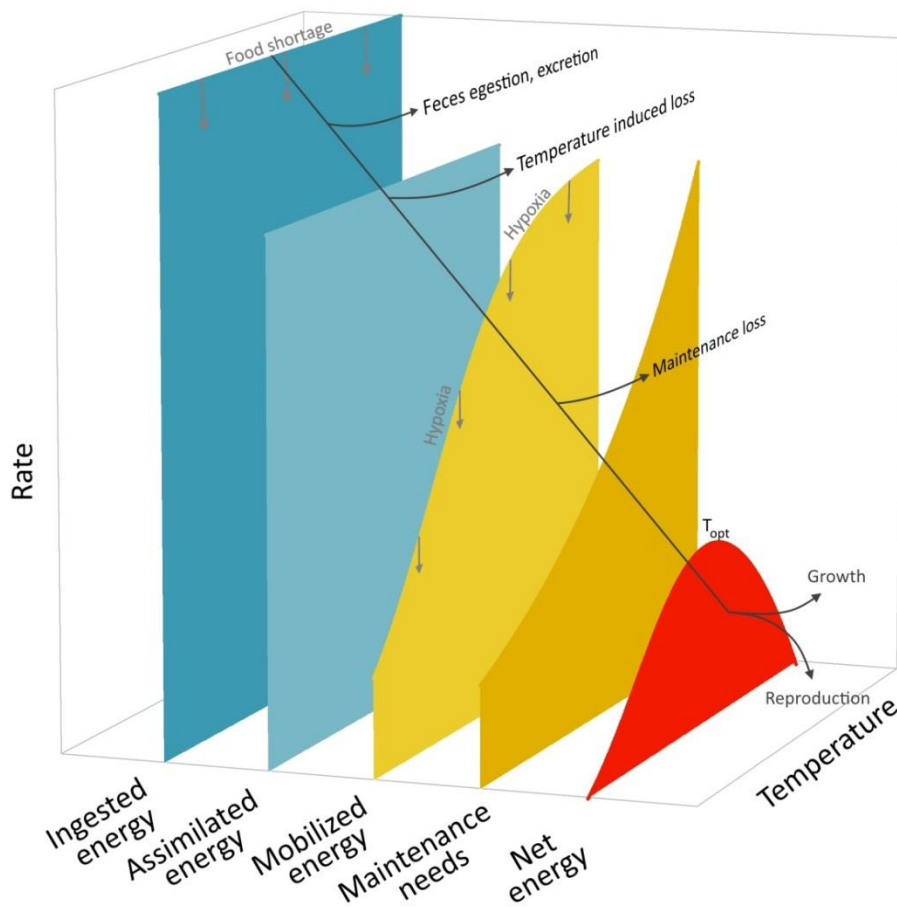
217 with ε_m the activation energy for the increase of the maintenance rate with temperature.

218 2.1.5. Net energy available for new tissue production

219 The net energy available for new tissues production E_P is the difference between the mobilized
220 energy E_M and the maintenance costs E_m defined as follows:

$$221 \quad E_P(i, t) = E_M(i, t) - E_m(i, t). \quad (9)$$

222 Given that the mobilized energy rate E_M increases at a lower rate than the maintenance rate E_m
223 close to the species preferred temperature, it results that, all other things being equal, the emerging
224 relationship between the net energy rate E_P (and thus somatic and gonadic growth, see next section)
225 and temperature is dome-shaped and conforms to the OCLTT theory and the principle of TPC (red
226 curve in Fig. 2).



227

228 Figure 2: Thermal responses of the bioenergetic fluxes from ingestion to tissue growth in Bioen-
 229 OSMOSE. The net energy rate dome-shaped curve (in red) conforms to the OCLTT theory and the
 230 principle of TPC. Food shortage impacts ingested energy and downstream fluxes. Hypoxia impacts
 231 mobilized energy and downstream fluxes. The maximum of the net energy rate (red curve) is called
 232 T_{opt} hereafter.

233 2.1.6. New tissue production: somatic and gonadic growth

234 The net energy E_P contributes to the production of new tissues with a proportion ρ being allocated
 235 to the gonadic compartment $g(i, t)$ and a proportion $(1 - \rho)$ to the somatic one $w(i, t)$. This
 236 proportion depends on the sexual maturity status $m(i, t)$ of the schools' individuals and their
 237 somatic mass $w(i, t)$. Before sexual maturation, i.e., when the maturity status $m(i, t) = 0$, ρ is equal
 238 to 0 and, after maturation, i.e., when $m(i, t) = 1$, ρ is determined such that the annual mean
 239 gonado-somatic index of individuals $\frac{g(i, t)}{w(i, t)}$ is constant throughout their adult life-stage and equal to r
 240 (Boukal et al., 2014; Lester et al., 2004; Quince et al., 2008):

$$241 \quad \rho(i, t) = m(i, t) \frac{r}{\eta \overline{E_P}(i)} w(i, t). \quad (10)$$

242 where, η is the ratio of energy density between somatic and gonadic tissues,
 243 $\overline{E_P}(i) = \frac{\Delta t}{a(i, t)} \sum_{t'=0}^{t'=a(i, t)/\Delta t} E_P(i, t')$ is the average net energy available per time step to individuals of
 244 school i since their birth, with Δt being the duration of a time step. Eq. 10 differs from a
 245 deterministic continuous time version of the same model (Boukal et al., 2014; Lester et al., 2004;
 246 Quince et al., 2008) where the current net energy $E_P(i, t)$ would be used instead of the average
 247 $\overline{E_P}(i)$. The averaging in a stochastic discrete time individual-based model such as Bioen-OSMOSE
 248 ensures a smooth increase of the proportion ρ as individuals grow by dampening strong variations in
 249 $E_P(i, t)$ and thus in $\rho(i, t)$ due to the stochasticity of prey encounters and hence of the ingested
 250 energy $I(i, t)$.

251 According to the definition of ρ , all net energy E_P is allocated to somatic growth before maturation
 252 and it is shared between somatic and gonadic growth after, with the proportion ρ allocated to
 253 gonads increasing with somatic mass (Boukal et al., 2014), which limits somatic growth as individuals
 254 become bigger. In case the mobilized energy E_M cannot cover the maintenance costs E_m , i.e., when
 255 $E_P < 0$, new tissue production is not possible and the gonadic compartment $g(i, t)$ is resorbed to
 256 provide energy for sustaining maintenance. Somatic growth is then defined as follows:

$$257 \quad \frac{dw}{dt}(i, t) = \begin{cases} (1 - \rho(i, t)) E_P(i, t) & \text{if } E_P(i, t) \geq 0 \\ 0 & \text{otherwise} \end{cases} \quad (11)$$

258 and gonadic growth as:

$$259 \quad \frac{dg}{dt}(i, t) = \begin{cases} \eta \rho(i, t) E_P(i, t) & \text{if } E_P(i, t) \geq 0 \\ \eta E_P(i, t) & \text{if } -g(i, t) \leq \eta E_P(i, t) < 0 \\ -g(i, t) & \text{if } \eta E_P(i, t) < -g(i, t) < 0 \end{cases} \quad (12)$$

260 where the second and third conditional formulas account for maintenance coverage by energy
 261 reserves contained in gonads. In the former case, gonads' energy can fully cover maintenance costs
 262 but in the latter it cannot, so that individuals undergo energetic starvation and incur additional
 263 starvation mortality (see Supporting Information S3).

264 2.1.7. Maturation

265 Age and size at maturation vary strongly between individuals due to phenotypic plasticity. This
 266 plasticity in maturation is modeled by a deterministic linear maturation reaction norm (LMRN) that
 267 represents all the age-length combinations at which an individual can become mature (Stearns, 1992;
 268 Stearns & Koella, 1986). In this framework, individuals become sexually mature when their growth
 269 trajectory in terms of body length intersects the LMRN. The maturity status $m(i, t)$ of individuals of
 270 school i at time step t is thus described as:

$$271 \quad m(i, t) = \begin{cases} 0 & \text{if } L(i, t) < m_0 + m_1 a(i, t) \text{ (immature)} \\ 1 & \text{if } L(i, t) \geq m_0 + m_1 a(i, t) \text{ (mature)} \end{cases} \quad (13)$$

272 with m_0 and m_1 the intercept and slope of the LMRN, respectively.

273 2.1.8. Reproduction

274 Mature individuals spawn during the breeding season, then a gonad portion is used to release eggs,
 275 what is represented by a gonad portion released $sp(t')$ above 0. The sex-ratio is assumed to be 1:1
 276 for all species and the number of eggs produced by school i at time t is defined as follows:

$$277 \quad N_{eggs}(i, t) = sp \left(t \bmod \frac{365}{\Delta t} \right) N(i, t) \frac{g(i, t)}{2w_{egg}} \quad (14)$$

278 with $t \bmod \frac{365}{\Delta t}$ giving the time of the year at time step t for a time step size of Δt , and w_{egg} the
 279 mass of an egg.

280 At each time step t of the breeding season (i.e., t for which $sp\left(i, t \bmod \frac{365}{\Delta t}\right) > 0$), $n_{s(i)}$ new
281 schools are produced by species $s(i)$, with the number of eggs, and thus individuals, per new school
282 i' calculated as follows:

$$283 \quad N(i', t) = \frac{\sum_{j|s(j)=s(i)} N_{eggs}(j, t)}{n_{s(i)}} \quad (15)$$

284 with $\sum_{j|s(j)=s(i)} N_{eggs}(j, t)$ the total number of eggs produced by schools of species $s(i)$ at time step
285 t , age of offspring set to 0, $a(i', t) = 0$, their somatic mass to the mass of an egg, $w(i', t) = w_{egg}$,
286 and their gonadic mass to 0, $g(i', t) = 0$. The new schools are released randomly depending on the
287 specific larvae habitat map.

288 2.1.9. Mortality

289 At each time step, a school experiences several mortality sources. The total mortality of a school i is
290 the sum of predation mortality caused by other schools, starvation mortality, fishing mortality, and
291 additional mortalities (i.e. larval, senescence, diseases, and non-explicitly modeled predators). For a
292 school i , the starvation mortality results from the encountered food, the environmental abiotic
293 variables and its maintenance rate. If the mobilized energy E_M covers the maintenance costs E_m ,
294 there is no starvation. However, if the mobilized energy E_M is lower than the maintenance costs, the
295 school i has an energetic deficit. In this case, the gonad $g(i, t)$ is used as a reserve. In case the gonad
296 content does not cover the exceeding maintenance costs, the school i faces starvation mortality
297 proportionally to the remaining energetic deficit. The equations and details about all mortality
298 processes are in Supporting Information S3.

299 **Table 1:** Variables and functions of the bioenergetics and life-history sub-models. (Δt :time step duration)

Symbol	Description	Units	Equations
Entities: Fish schools			
Ontogenic state			
<i>State variables</i>			
$a(i, t)$	Age of school i 's individuals at time step t	y	3, 13
$w(i, t)$	Somatic mass of school i 's individuals at time step t	g	2, 7, 10,11
$g(i, t)$	Gonadic mass of school i 's individuals at time step t	g	12, 14
<i>Emerging individual variables</i>			
$L(i, t)$	Total length of school i 's individuals at time step t	cm	1,13
$m(i, t)$	Maturity state of school i 's individuals at time step t	–	10, 13
$a_m(i)$	Maturation age of school i 's individuals	y	
$w_m(i)$	Maturation somatic mass of school i 's individuals	g	
$L_m(i)$	Maturation length of school i 's individuals	cm	
$N_{eggs}(i, t)$	Total fecundity of school i at first time step t of the breeding season	#	14, 15
<i>Abundance: State variable</i>			
$N(i, t)$	Number of individuals in school i at time step t	#	1, 14,15
$B(i, t)$	Biomass of school i at time step t	g	1
<i>Spatial Location: State variable</i>			
$c(i, t)$	Grid cell of school i at time step t	–	1
<i>Taxonomic identity: State variable</i>			
$s(i)$	Species to which school i belongs	–	
Bioenergetics			
<i>Emerging individual variables</i>			
$P(i, t)$	Available prey biomass to an individual of school i at time step t	g	1, 2
$\psi(i, t)$	Life-stage dependent multiplicative factor of maximum mass-specific ingestion rate of school i at time step t	–	2, 3

$I(i, t)$	Ingestion rate of individuals in school i at time step t	$g \cdot \Delta t^{-1}$	2, 4
$E_M(i, t)$	Mobilized energy rate of individuals of school i at time step t	$g \cdot \Delta t^{-1}$	4, 9
$E_m(i, t)$	Maintenance cost rate of individuals of school i at time step t	$g \cdot \Delta t^{-1}$	7, 9
$E_P(i, t)$	Net energy available for new tissue production	$g \cdot \Delta t^{-1}$	9, 10, 11, 12
$\rho(i, t)$	Proportion of net energy allocated to gonadic growth	–	10, 11, 12
$\frac{dw}{dt}(i, t)$	Somatic growth rate	$g \cdot \Delta t^{-1}$	11
$\frac{dg}{dt}(i, t)$	Gonadic growth rate	$g \cdot \Delta t^{-1}$	12
<i>Functional responses</i>			
$f(P)$	Holling's type 1 functional response to prey biomass P	–	2
$\lambda([O_2])$	Dose-response function of energy mobilization to dissolved oxygen concentration $[O_2]$	–	4, 5
$\varphi_M(T)$	Response of energy mobilization to temperature T	–	4, 6
$\varphi_m(T)$	Response of maintenance rate to temperature T	–	7, 8
Spatial scales and units: grid cells			
Spatial coordinates: <i>State variables</i>			
$x(c)$	Longitude of grid cell c		
$y(c)$	Latitude of grid cell c		
Physico-chemical factors: <i>State variables</i>			
$pc_k(c, t, z)$	Value of physico-chemical factor k of grid cell c at time step t of layer z		
$T(c, t)$	Temperature of grid cell c at time step t	K	4, 6, 7, 8
$[O_2](c, t)$	Dissolved O_2 concentration of grid cell c at time step t	%	4, 5
Biomass of LTL: <i>State variables</i>			
$B_{LTL}(c, j, t)$	Biomass of <i>LTL</i> group j of grid cell c at time step t	g	

300 **Table 2:** Species- specific parameters of the bioenergetic and life-history sub-model. (Δt : time step duration). One parameter is constant across species,
 301 namely the Boltzmann constant ($k_B = 8.62 \cdot 10^{-5} \text{ eV} \cdot \text{K}^{-1}$).

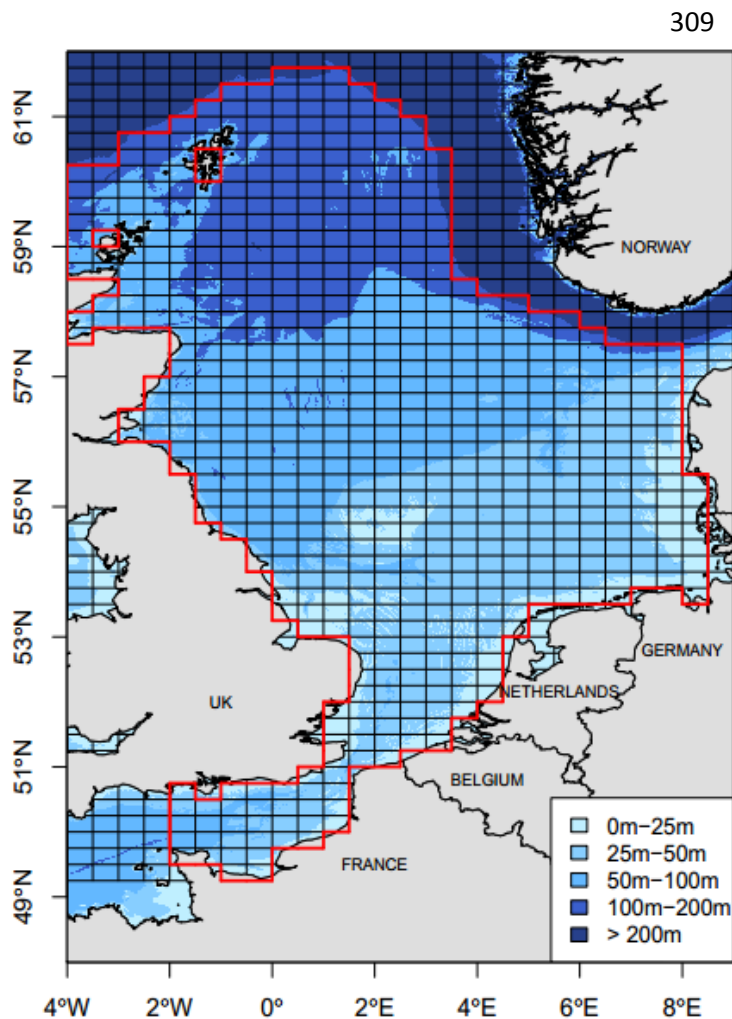
Symbol	Description	Units	Equations	Source
Ingestion, assimilation and mobilization				
R_{min}, R_{max}	Minimum and maximum predator to prey size ratio	–	1	Literature
$\gamma(i, j)$	Accessibility coefficient of prey species $s(j)$ to predator species $s(i)$ according to life stage	–	1	Literature
I_{max}	Maximum mass-specific ingestion rate	$g \cdot g^{-\beta} \cdot \Delta t^{-1}$	2	Calibrated
β	Scaling exponent of maximum ingestion rate and maintenance rate with body mass	–	2, 7	Assumed
θ	Multiplicative factor of maximum mass-specific ingestion rate at larval stage	–	3	Estimated ¹
a_l	Age at the end of the fast growth period	y	3	Literature
ξ	Assimilation efficiency	–	4	Literature
$c_{O,1}$	Asymptote of energy mobilization dose-response function to dissolved oxygen saturation	–	5	Estimated ²
$c_{O,2}$	Slope of energy mobilization dose-response function to dissolved oxygen saturation	%	5	Estimated ²
ε_M	Increasing activation energy of the energy mobilization temperature function	eV	6	Estimated ³
ε_D	Declining activation energy of the energy mobilization temperature function	eV	6	Estimated ³
T_p	Temperature of peak value in energy mobilization	K	6	Estimated ³
Φ	Normalization constant of the energy mobilization temperature function	–	6	Estimated ³
Maintenance				
c_m	Mass-specific maintenance rate	$g \cdot \Delta t^{-1}$	7	Literature
ε_m	Activation energy of the maintenance temperature function	eV	8	Estimated ³
Maturation				
m_0	Intercept of the maturity reaction norm	cm	13	Estimated ¹
m_1	Slope of the maturity reaction norm	cm · y ⁻¹	13	Estimated ¹
New tissue production				
η	Energy density ratio between somatic and gonadic tissue	–	10, 12	Literature

k	Allometric length-somatic mass relationship coefficient	$g \cdot cm^{-\alpha}$		Estimated ⁴
α	Allometric length-somatic mass relationship exponent	–		Estimated ⁴
Reproduction				
r	Gonado-somatic index	–	10	Estimated ¹
w_{egg}	Egg mass	g	14	Estimated ⁵
$sp(t)$	Spawning seasonality expressed as a fraction of the gonad energy available at the time step t	–	14	Literature
$n_{s(i)}$	Number of new schools produced at each time step of the breeding season for the species s of school i	#	15	Arbitrary

- 302 ¹ from Size Maturity Age Length Key (SMALK) data (see Supporting Information S2.1)
- 303 ² from ecophysiological data (see Supporting Information S2.4)
- 304 ³ from a combination of SMALK and thermal tolerance data (see Supporting Information S2.3)
- 305 ⁴ from length-mass data
- 306 ⁵ from fecundity data (see Supporting Information S2.5)

307 2.2. Application to the North Sea ecosystem: Bioen-OSMOSE-NS

308 2.2.1. Area and explicit species



The Bioen-OSMOSE-NS area includes the North Sea (ICES area 4) and the eastern English Channel (ICES area 7d), excluding the area deeper than 200m (notably the Norwegian Trench), and extends from 49° N to 62° N and from 4° W to 8.5° E (red delimitation in Fig. 3). The model covers the area by 632 regular cells of 0.25° x 0.5°. 16 HTL species are modeled explicitly, accounting for 89% of the total fisheries landings in the area over the period 2010-2017 (ICES 4abc and 7d) and more than 90% of the scientific

North Sea International Bottom Trawl Survey (NS-IBTS-Q1, DATRAS) catches. There are five pelagic species, seven demersal species, three benthic flatfish and one shrimp functional group. The species and their input parameters are listed in Supporting Information S4, Table S3, and the data sources, references, and/or methodology to estimate these parameters are presented in the Supporting Information S6. The species spatial distributions are described by presence/absence maps, and informed per life stages (egg-larvae, juvenile, and adult) whenever information was available (Supporting Information S7). As individuals are represented in a 2D horizontal environment, a predator-prey accessibility matrix T , used to determine the accessibility coefficient $\gamma(i, j)$ (see Eq. 1 and Table 2), is defined according to the vertical distribution overlap between potential predator and prey species possibly per life stage (Supporting Information S4, Table S5). The gonad portion released $sp(t)$ is estimated from the seasonality of eggs' release (see Supporting Information S2.5). The

328 North Sea International Bottom Trawl Survey (NS-IBTS-Q1, DATRAS) catches. There are five pelagic
329 species, seven demersal species, three benthic flatfish and one shrimp functional group. The species
330 and their input parameters are listed in Supporting Information S4, Table S3, and the data sources,
331 references, and/or methodology to estimate these parameters are presented in the Supporting
332 Information S6. The species spatial distributions are described by presence/absence maps, and
333 informed per life stages (egg-larvae, juvenile, and adult) whenever information was available
334 (Supporting Information S7). As individuals are represented in a 2D horizontal environment, a
335 predator-prey accessibility matrix T , used to determine the accessibility coefficient $\gamma(i, j)$ (see Eq. 1
336 and Table 2), is defined according to the vertical distribution overlap between potential predator and
337 prey species possibly per life stage (Supporting Information S4, Table S5). The gonad portion released
338 $sp(t)$ is estimated from the seasonality of eggs' release (see Supporting Information S2.5). The

339 seasonality of eggs' release data are taken from the literature and presented in Supporting
340 Information S8. The fishing mortality rates are size-dependent due to fisheries size-selectivity. The
341 calibrated maximum fishing mortality rates F_{max} are in Supporting Information S4, Table S3. The
342 species-specific fishing selectivity curves are in Supporting Information S11. The larval and additional
343 mortality are in Supporting Information S4, Table S3.

344 2.2.2. Forcing variables: low trophic levels and physical variables

345 The Bioen-OSMOSE model is forced by temperature and oxygen variables and by LTL biomass fields.
346 The forcing data come from the regional biogeochemical model POLCOMS-ERSEM applied to the
347 North Sea ecosystem (Butenschön et al., 2016). The modeled period is 2010-2019. There are five
348 pelagic (micro-phytoplankton, diatoms, heterotrophic flagellates, micro-zooplankton, meso-
349 zooplankton) and three benthic (suspension feeders, deposit feeders and meiobenthos) LTL groups
350 (Supporting Information S5): the biomass of the former is available in three dimensions and
351 therefore integrated vertically, while the biomass of the latter is available in two-dimensions. Two
352 other groups of large and very large benthos are set as homogeneous prey fields in space and time
353 due to the absence of data and model output for these LTL groups. For the temperature and oxygen
354 variables, their values are integrated over the 43 vertical layers of POLCOMS-ERSEM to force pelagic
355 and demersal HTL species. Only the values in the deepest layer are used for benthic species. Monthly
356 maps for each LTL group and temperature and oxygen variables are shown in Supporting Information
357 S9.

358 2.2.3. Calibration

359 The model is calibrated, i.e., parameters for which an independent estimator is unavailable are
360 estimated, using maximum likelihood estimation based on an optimization method adapted to high-
361 dimensional parameter space, namely an evolutionary algorithm available in the package calibraR in
362 R (Oliveros-Ramos & Shin, 2016). The algorithm explores the space of unknown parameters (referred
363 to as "calibrated" in Supporting Information S4, Table S3) so as to maximize the likelihood obtained
364 by comparing model outputs to observed data. Data used to calibrate Bioen-OSMOSE-NS are
365 fisheries landings (ICES, 2019a), size-at-age from scientific surveys (NS-IBTS-Q1, North Sea
366 International Bottom Trawl Survey (2010-2019), available online at <http://datras.ices.dk>) and
367 estimated biomasses for assessed species (ICES, 2016, 2018a, 2018b, 2018c, 2019b). The discard rate
368 of assessed species is low except for dab and plaice: the data used as landings and biomass for these
369 species includes estimated discards from stock assessments. The biomasses estimated for stocks
370 entirely located within the study area are directly used (herring, sandeel, sprat, sole, and whiting).
371 For stock with a wider distribution than the study area, the biomass data is taken proportional to

372 total stock biomass according to the ratio between landings in the study area and total landings
373 (mackerel, norway pout, plaice, saithe, cod, haddock, dab, hake). There is no biomass target value for
374 unassessed species (horse mackerel, grey gurnard, hake, shrimp). The calibration is performed for an
375 average state of the ecosystem for the period 2010-2019 by using observed data averaged over the
376 period as target values (Supporting Information S10). The calibration is run using four phases with a
377 new set of parameters to be estimated added at each phase for better convergence of the
378 optimization: the first phase calibrates the LTL group accessibility coefficients only (Supporting
379 Information S5), the larval mortalities are added for the second phase (Supporting Information S4,
380 Table S3), the maximum ingestion I_{max} rates are added on phase three (Supporting Information S4,
381 Table S3), and the maximum fishing mortality rates and the additional mortality rates are added in
382 the last phase (Supporting Information S4, Table S3).

383 The calibrated configuration is run for 80 years. The first 70 years is the spin-up period, a period
384 during which the system stabilizes. The results presented hereafter are the years after the spin-up
385 period. 28 replicates of the model are run with the same parameterization to account for Bioen-
386 OSMOSE stochasticity.

387 **3. Results and discussion**

388 In this paper, we present the Bioen-OSMOSE framework with its first application to the North Sea
389 ecosystem, involving the coupling of the POLCOMS-ERSEM model for the physical and LTLs model
390 with the HTLs Bioen-OSMOSE model. The North Sea trophic network has been intensively studied
391 and modeled, either considering the whole ecosystem (Blanchard et al., 2014; Cormon et al., 2016;
392 Heath, 2012; Lewy, 2004; Mackinson & Daskalov, 2007) or part of it (including the English Channel)
393 (Girardin et al., 2018; Stäbler et al., 2016; Travers-Trolet et al., 2019).

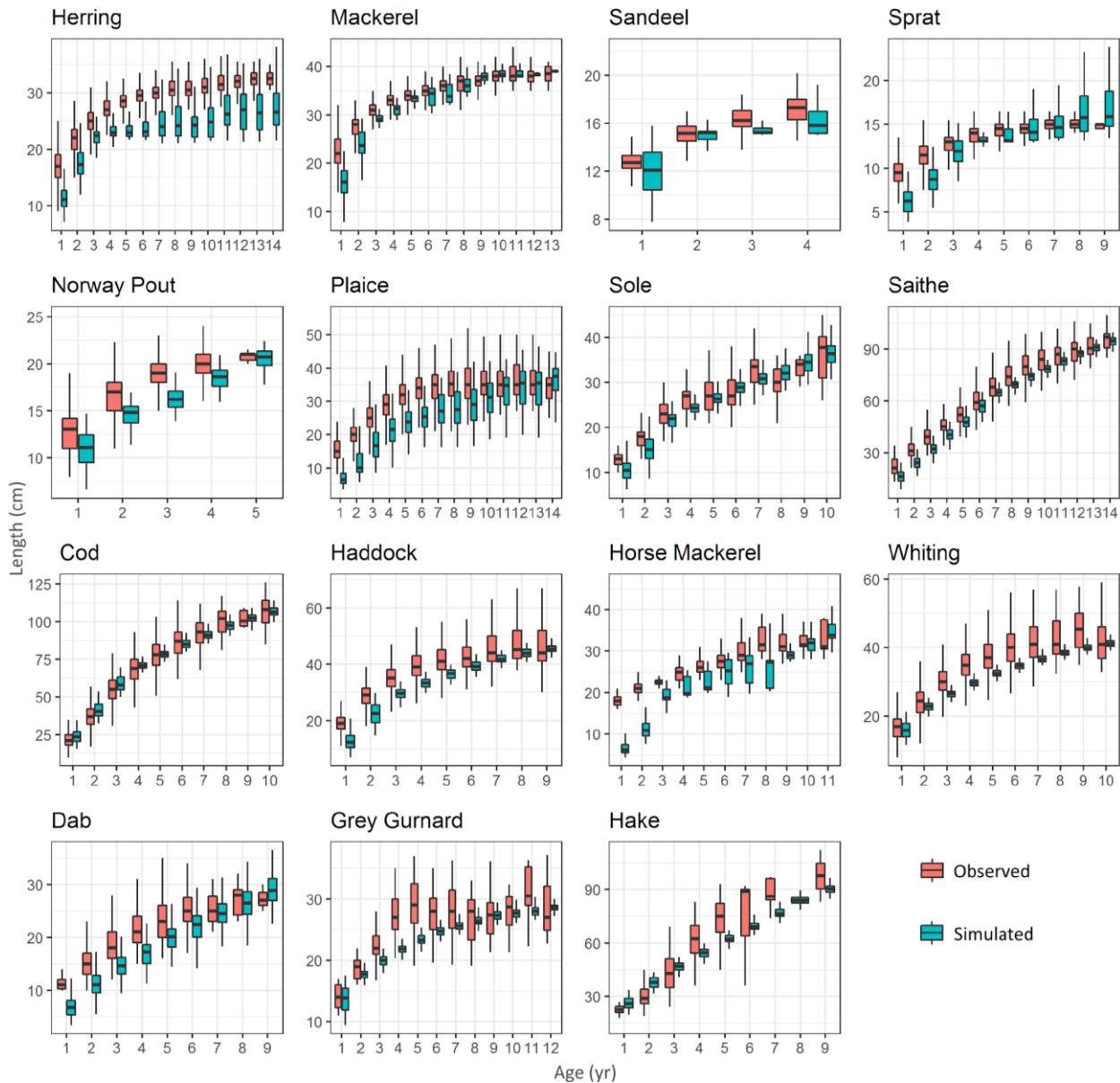
394 This is the first time that the Bioen-OSMOSE model is used, i.e the OSMOSE model (Shin & Cury,
395 2004) augmented with a mechanistic description of the emergence of life history from underlying
396 bioenergetics and its response to temperature and oxygen seasonal and spatial variations. It is also,
397 to our knowledge, the first application of a marine ecosystem model considering the impacts of
398 physiologically-induced trait changes in response to food, oxygen, and temperature at the individual,
399 population, and community levels.

400 **3.1. Model evaluation**

401 The calibration procedure allowed us to estimate unknown parameters to obtain a model
402 configuration that fairly accurately represents the North Sea ecosystem. Particular attention was paid

403 to obtaining satisfactory results for indicators at different biological levels, the final result being a
404 compromise between indicators used as target (size-at-age, catch and biomass) and emerging
405 variables (maturation and diet).

406 3.1.1. The individual level: size structure and maturity ogives



407
408 Figure 4: Boxplot of size-at-age per species for observed (pink) and simulated (blue) individual data.
409 Horizontal bars represent the first, second and third quartiles. The whiskers' extremities represent
410 1.5 times the interquartile space (the distance between the first and third quartile). The shrimp
411 group was not represented in this graph, as available observed data are not sufficiently
412 taxonomically resolved to be relevant for this functional group.

413 The simulated mean sizes-at-age correctly reproduce the observed ones (Fig. 4), supporting the
414 credibility of the growth process described by the new bioenergetic sub-model. The Von-Bertalanffy-
415 like shape and the indefinite growth are two realistic properties reproduced with our model. As
416 observed in the data, it can be noted that growth is faster during the first years of life and the sizes at
417 older ages slowly tend to an infinite size. The simulated and observed sizes-at-age interquartile
418 ranges overlap for almost all age classes of the species. The simulated size hierarchy between species
419 is consistent with the observed one, which is a key expected property for a size-based model.

420 The simulated sizes-at-age 1 have generally the poorest fit to observed data. Size-at-age class 1 partly
421 inherits uncertainties linked to size at hatching and to the growth rate at very early stages, notably
422 the larval one, that is imperfectly accounted for by the multiplicative factor of maximum mass-
423 specific ingestion rate for the larvae at larval stage θ . In addition, growth during the first year is
424 mainly driven by food limitation implying that the size-at-age class 1 is the result of a complex model
425 adjustment between growth rate, competition and prey accessibility.

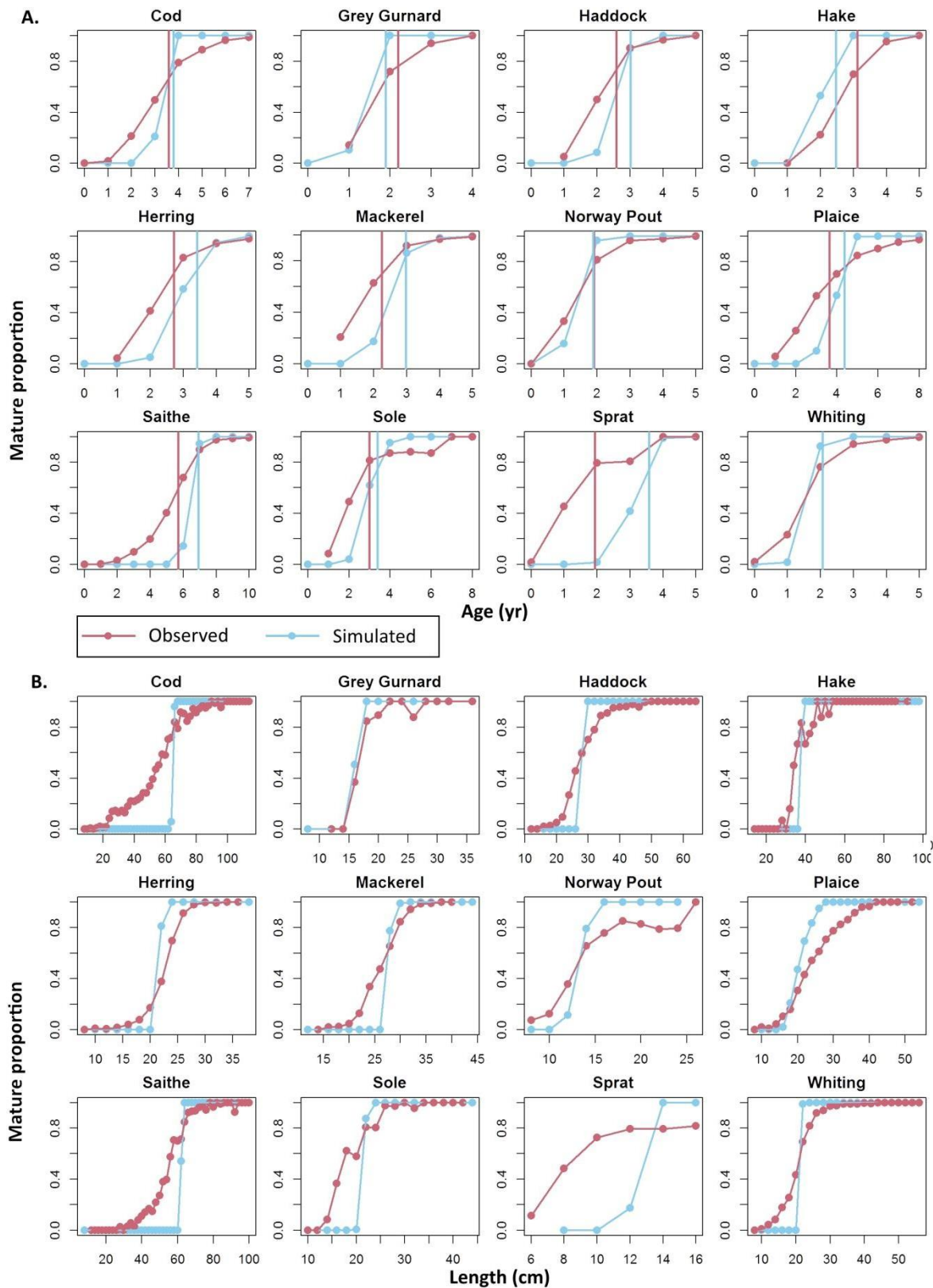
426 The variance in size-at-age differs between observed and simulated data, mainly for demersal
427 species. The observed variance in sizes-at-age is the result of macro-environmental variations, i.e. in
428 the abiotic environment (Brown et al., 2004; Gislason et al., 2010; Thomas et al., 2019) and food
429 availability (Brosset et al., 2016), micro-environmental variations, i.e., in undetectable or
430 unaccounted for environmental conditions, and genetic variability in energy allocation inducing
431 variability in size-at-age (Enberg et al., 2012). In contrast, the variance of simulated size-at-age only
432 results from macro-environmental variations. Thus, the species with observed variance higher than
433 the simulated variance is because genetic and micro-environmental variances are not modeled here.

434 Comparison of observed and simulated age and size maturity ogives demonstrate the ability of
435 Bioen-OSMOSE to correctly reproduce maturation patterns (Fig. 5). The simulated mean age at first
436 maturation perfectly matches that observed for three species (cod, norway pout, and whiting). In
437 observed data, age is given with yearly resolution. Therefore, we consider that a correct pattern is
438 obtained for seven additional species for which the difference between simulated and observed age
439 at maturity is less than one year (grey gurnard, haddock, hake, herring, mackerel, plaice and sole).
440 The worst deviation is obtained for sprat and saithe with simulated maturation occurring at later ages
441 and larger sizes than that observed. Saithe and sprat have lower mean sizes at early ages than
442 observed ones (Fig. 4) which can explain the late simulated maturation. However, both species have
443 simulated maturation ages that stand within observed ranges, being lower than the upper bounds of
444 observed maturation ages, namely 9 years for saithe in the North Sea (Cohen et al., 1990) and 4 years

April 20, 2022

445 for sprat (Ojaveer and Aps, 2003) in the Baltic Sea (only mean values were reported for the North Sea
446 population).

447 The use of LMRNs improves the description of the variability in the maturation process compared to
448 the use of fixed age or size at maturity, as is most commonly done in marine ecosystem models, such
449 as previously in the OSMOSE framework (Shin & Cury, 2004) or in other models (Audzijonyte et al.,
450 2019). Consequently, individuals from the same size or age class do not necessarily have the same
451 maturity state (Fig. 5), which increases the realism of the life cycle description. For the majority of
452 the species, the slope of simulated age and size maturity ogives is higher than the observed one,
453 meaning that the observed maturation process is more variable than in simulations. As for size-at-
454 age, part of the observed variability in maturation is determined by genetic and/or micro-
455 environmental variability (Law, 2000; van Wijk et al., 2013) and is not modeled here.



456 Figure 5: Age (A) and size (B) maturity ogives per species for observed (pink) and simulated (blue) data.
 457 Results are shown for species for which there is enough data to estimate and plot the observed age
 458 and size maturity ogives. Age data have a yearly resolution and size data a 2-centimeter resolution. The
 459 simulated (blue) and observed (pink) mean age at maturity are represented by vertical lines (A). The

460 mean size at maturity is not represented. The observed size maturity ogive is not strictly increasing and
461 does not allow a reliable estimation of the maturation size.

462 3.1.2. The population level: fisheries catches and species biomass

463 Given the high statistical confidence in catch data, a greater weight was given to the corresponding
464 likelihood component in the calibration process which resulted in reaching targets, i.e., simulated
465 catches were within the range of observed values, for the majority of species (Fig. 6A). Plaice and dab
466 are the two species for which the simulated catches were the farthest from their targets. Plaice and
467 dab are two by-catch species that are largely discarded. These discards are estimated to be up to
468 40% for plaice and 90% for dab (ICES, 2018c). The catch data used as target here is reconstructed
469 from the landings and discards estimates, which, in case of overestimation of discards, could explain
470 the discrepancy between the target and the simulated values. The poor fit of plaice could also be
471 partially explained because the migrations between the Eastern and Western English Channel stocks
472 are not taken into account in Bioen-OSMOSE-NS (ICES, 2021).

473 The simulated biomasses are within acceptable ranges (Fig. 6B) and the resulting dominance ranking
474 between species groups respects the ranking based on stock assessment estimations: small pelagic
475 fish are the dominant group with herring as the main species. Demersal species have lower
476 biomasses with saithe and haddock as the most abundant ones. Flatfish are the minority group in the
477 system, which is dominated by plaice.

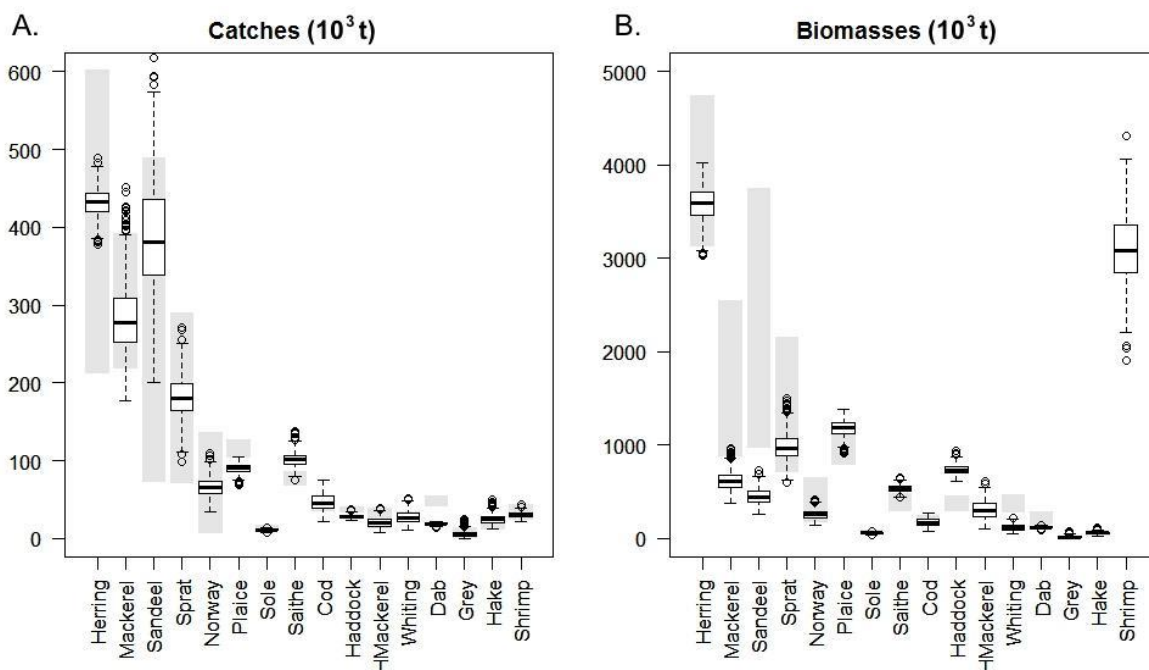
478 The simulated biomasses of mackerel and sandeel are underestimated compared to the stock
479 assessment biomass estimates (Fig. 6B). Mackerel is a widely distributed stock in the North East
480 Atlantic area and our biomass estimate in the North Sea (proportional to the total biomass in the
481 North East Atlantic according to the ratio between North Sea landings and total landings) relies on
482 the assumption of a uniform fishing effort in the assessed area. A higher fishing effort within the
483 North Sea would lead to an overestimation of the target biomass for the area, which is credible since
484 the North Sea is a historically heavily fished area. An ecopath model of the North Sea (Mackinson &
485 Daskalov, 2007) also estimated a lower biomass for this species (980 400 t). Underestimation for
486 sandeel is more troublesome as it is a key forage species in the North Sea (Engelhard et al., 2014), for
487 which the stock assessment is considered to be very detailed with 7 stocks in the area (ICES, 2016).
488 The fact that the Bioen-OSMOSE-NS model does not describe the peculiar overwintering behavior of
489 this species, which buries itself in sand and thus is less vulnerable to fishing and predation in winter
490 (Henriksen et al., 2021), may explain the underestimation of its biomass. The sandeel may also be

April 20, 2022

491 over-consumed by higher trophic level species in our model, indicating a missing forage species or an
492 over-consumption of sandeel over LTL forced prey.

493 In Bioen-OSMOSE-NS, flatfish are represented by only the three main species of the North Sea
494 ecosystem. However, there are other flatfish species each with low biomass levels (*Scophthalmus*
495 *maximus*, *Microstomus kitt*, *Scophthalmus rhombus*, *Platichthys flesus*...) (NS-IBTS-Q1, DATRAS, Piet
496 et al., 1998) but whose total biomass is not negligible (NS-IBTS-Q1, DATRAS, Mackinson & Daskalov,
497 2007). Thus, the overestimation of plaice biomass may compensate for the absence of these other
498 flatfish in the model that may leave an empty trophic niche.

499 The high biomass of the shrimp functional group, dominated in the ecosystem by the species
500 *Crangon crangon* and *Pandalus borealis*, may seem surprising. However, as the micro- and meso-
501 zooplankton groups described by the biogeochemical model POLCOMS-ERSEM represent pelagic
502 prey of sizes smaller than 0.5 cm only, we suggest that the shrimp functional group has a broader
503 ecological role in the Bioen-OSMOSE-NS model by actually representing all LTL prey larger than 0.5
504 cm in the water column, whose biomass is critical to sustain the food web. These prey include
505 demersal crustaceans with diel vertical migration such as *Crangon crangon* or *Pandalus borealis* as
506 well as more pelagic species such as large amphipods (large *Bathyporeia elegans*) or euphausiids
507 (*Thysanoessa sp.*, *Meganyctiphanes norvegica*).



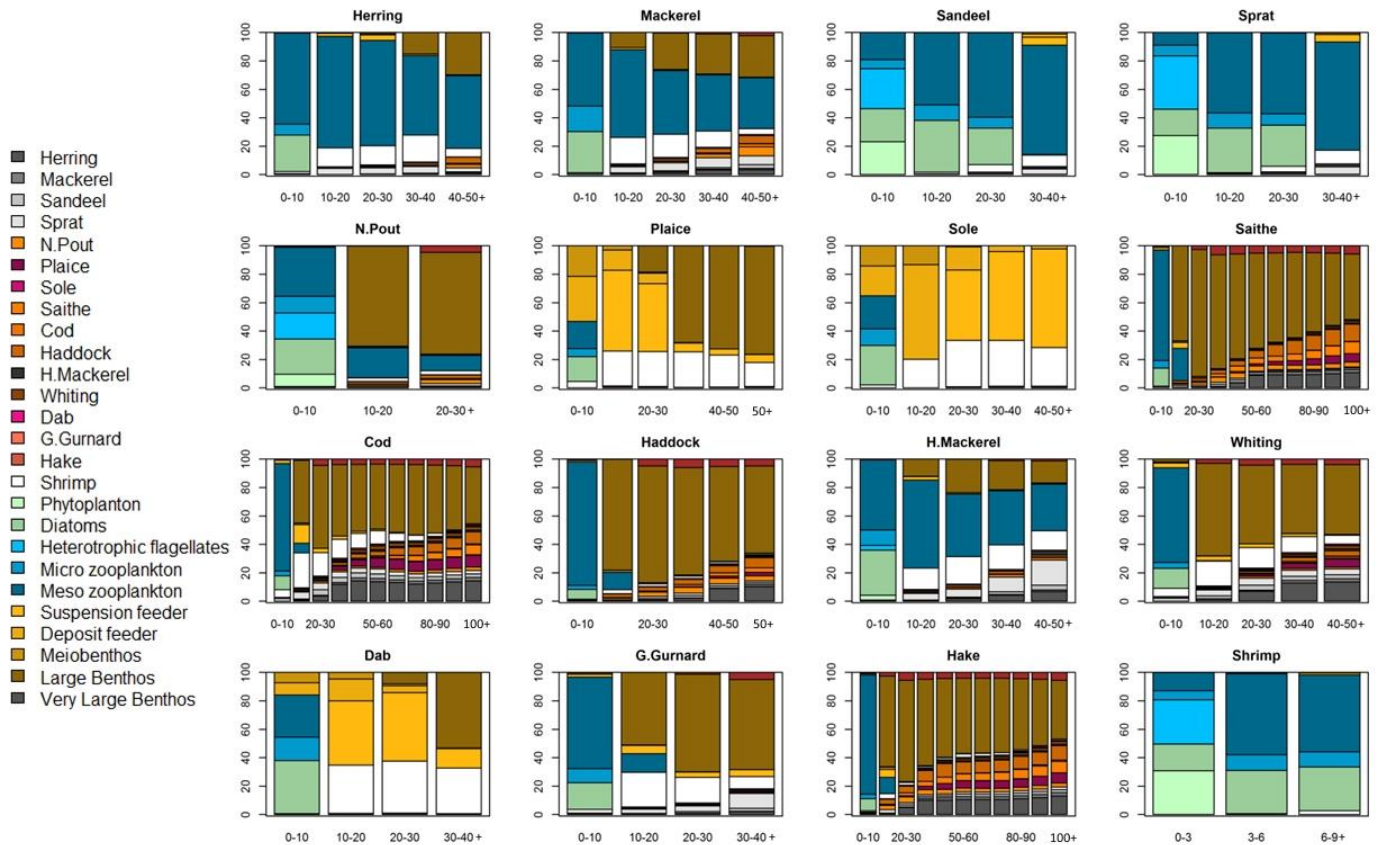
508

509 Figure 6: Fisheries catches (A) and biomasses (B), in thousand tons, per species for stock assessment
510 estimates and simulated data. The boxplots represent the simulated data for 28 replicated

26

511 simulations (stochastic model) for the catches and biomasses per species, with the first, second and
512 third quartiles represented horizontally in each plot. The gray bars show the minimal and maximum
513 values observed for catch and biomass estimates from stock assessment for the 2010-2019 period.
514 The species without gray bars for biomasses are not assessed in the area.

515 3.1.3. The community level: trophic diets



516

517 Figure 7: Diet in percent of biomass eaten of prey species per size class of the predator species in cm.
518 For each predator species, the last size class (x-axis) includes all the larger individuals.

519 In Bioen-OSMOSE, the diet emerging from opportunistic predation reflects the species' relative
520 abundances, their sizes and their spatio-temporal overlap. There are no pre-established predator-
521 prey diet matrix in the parameterization of the model so confronting the output diets to observed
522 ones, especially in terms of species composition, is a way to validate the model properties.

523 The simulated diets show patterns that are consistent with observations (Fig. 7). The model
524 reproduces correctly observed ontogenetic diet shifts (Timmerman et al., 2020). The prey
525 composition shifts between pelagic early-life stages (size class 0-10 cm for fish species and 0-3 cm for
526 the shrimp group) and the older life stages for all species. There are different emerging diet patterns

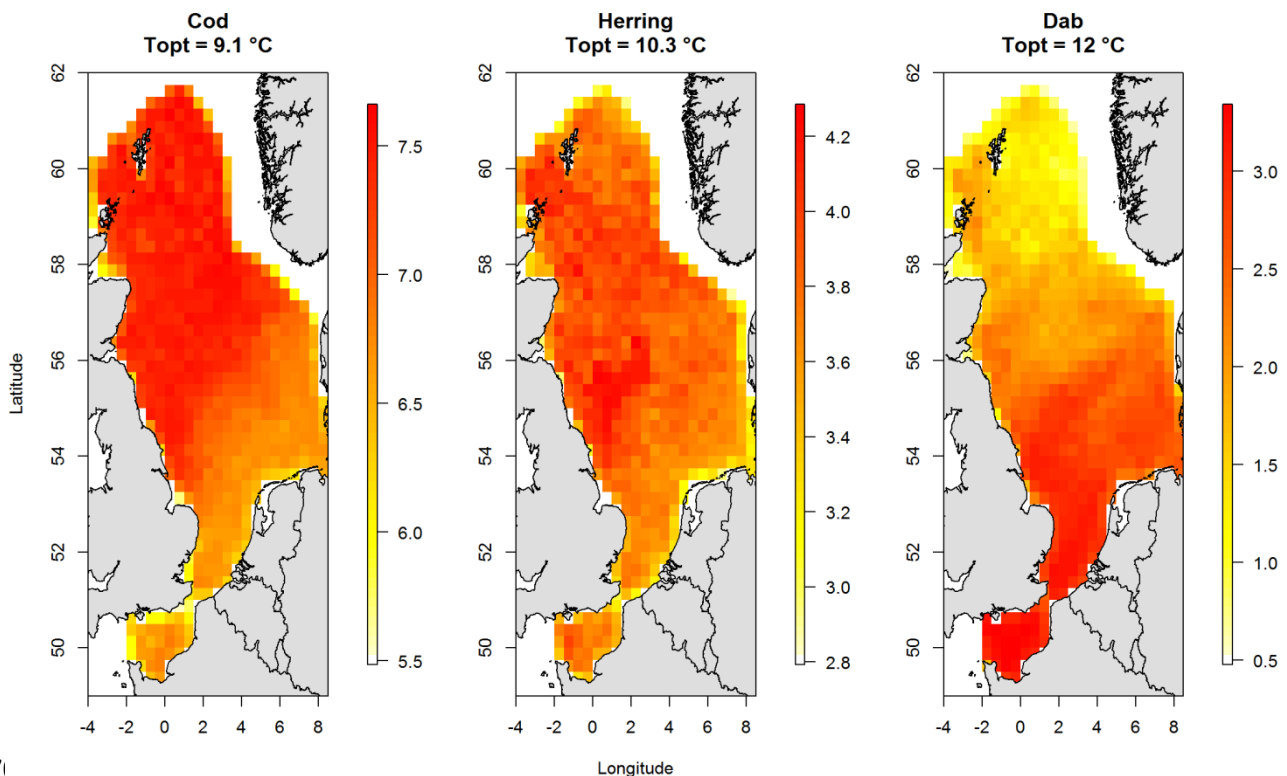
527 depending on the predator's position in the water column. The pelagic species diet is dominated by
528 phyto- and especially zoo-planktonic prey, which is consistent with studies on sprat and herring (De
529 Silva, 1973; Last, 1989; Raab et al., 2012). The benthic species diet is composed of benthic LTL groups
530 and the shrimp functional group, similarly to results obtained by an isotopic study (Timmerman et al.,
531 2021), by plaice and sole stomach content studies for adults (Rijnsdorp & Vingerhoed, 2001) and for
532 juveniles (Amara et al., 2001) with smaller prey for sole than for plaice and dab of the same size
533 (Amara et al., 2001). The demersal species have an intermediate diet composition with a high degree
534 of piscivory for the larger fish. There is a steady increase in piscivory with size, mainly for demersal
535 species, as shown empirically for whiting, cod, saithe and haddock in the area (Robb & Hislop, 1980;
536 Timmerman et al., 2020) but not for norway pout (Robb & Hislop, 1980). In addition, there is a
537 significant part of benthic prey in the pelagic species diet, which correctly represents the strong
538 pelagic-benthic coupling in this area (Giraldo et al., 2017; Timmerman et al., 2021): the pelagic
539 piscivorous fish (mackerel and horse mackerel) also feed on benthic prey which represents half of
540 their diet (Giraldo et al., 2017).

541 **3.2. The physiological level: spatial pattern**

542 New outputs and original questions emerge from the physiological responses of metabolic rates to
543 biotic and abiotic variables and can be explored with the Bioen-OSMOSE model. The representation
544 of emergent spatially and seasonally varying bioenergetic fluxes is an example of the new features
545 brought by Bioen-OSMOSE that can help improve our understanding of the relationship between
546 temperature and ecosystem dynamics, which is crucial in the context of global warming (Lindmark et
547 al., 2022). This spatial and seasonal variability of metabolism in relation to temperature variation is
548 often under-studied.

549 The simulated adult mean mass-specific net energy rate for new tissue production \bar{e}_p , is the ratio
550 between the population mean mass-specific net energy rate (see Eq. 9) and the weight at the
551 exponent β and it drives the energy allocated to growth and reproduction. It is spatially represented
552 as an output example (Fig. 8). This spatial representation of emerging bioenergetic fluxes highlights
553 the high variability of mean mass-specific net energy rate for three widely distributed species in the
554 North Sea ecosystem with contrasted thermal preferences: cod, herring and dab (quoted by
555 increasing physiological optimum temperature T_{opt} , defined in Fig. 2). The spatial pattern of mean
556 mass-specific net energy is mainly explained by species thermal preferences. The species with the
557 lowest thermal preference (cod) has a greater net energy acquisition in the northern part of the area
558 where the water is colder on average. The opposite pattern emerges for the species with the highest

559 thermal preference (dab). There is a better energy acquisition in the south where the average
560 temperature is higher than in the north. A similar spatial pattern for growth rate was predicted as
561 outputs of a single-species bioenergetic model for two thermophilic flatfish in the North Sea (Teal et
562 al., 2012). Herring, which has an intermediate thermal preference, exhibits a more spatially
563 homogeneous emerging mean mass-specific net energy rate. During the period described by our
564 model (2010-2019), temperature is the main driver of spatial variability in bioenergetic fluxes for
565 these three species. The spatial distribution of food has little or no impact on adult energy acquisition
566 for these examples as we observe that simulated food ingestion frequently reaches the maximum at
567 the adult stage (results not shown). Likewise, oxygen saturation has no impact on the emerging
568 spatial pattern because oxygen saturation is not low enough to become a primary driver of
569 bioenergetic fluxes (Vaquer-Sunyer & Duarte, 2008, Supporting Information S10).



571
572 Figure 8: Spatial variability of the mean adult mass-specific net energy rate available for new tissue
573 production, per model cell for cod, herring and dab. These three species are distributed over the
574 whole modeled area although they have different optimum temperatures T_{opt} . Cod, herring and dab
575 mean adult mass-specific net energy available rate for new tissue production averaged over the area
576 are 7.4, 3.3, and 2.7 $g \cdot g^{-\beta}$, respectively. Spatial variations of this bioenergetic flux can be driven by
577 temperature, oxygen and food variation.

577 4. Conclusion

578 Applying Bioen-OSMOSE to the North Sea allows demonstrating the feasibility of its parameterization
579 for several species with different levels of available knowledge and allows evaluating the framework
580 capabilities. Bioen-OSMOSE-NS simulates many different outcomes that convincingly reproduce
581 observations such as biomasses, catches, sizes at age, maturation ogives, and diets. The model also
582 produces compelling spatial responses of the bioenergetic fluxes to temperature variations.

583 The Bioen-OSMOSE framework is also intended to be used for hindcast or forecast simulations.
584 Hindcasting could help disentangling the effects of temperature increase and/or oxygen depletion on
585 the historical trends in life-history traits. Hindcasting with Bioen-OSMOSE could also be useful to
586 understand the contribution of temperature- and oxygen-induced physiological changes in
587 population and community dynamic alterations that were observed in past periods. Given the
588 increasing need to reliably forecast biodiversity under future climate change scenarios, we believe
589 that Bioen-OSMOSE will also allow improving projections of regional ecosystem dynamics by taking
590 into account future individual-level physiological changes and their consequences at the population
591 and community levels.

592 **Acknowledgements**

593 This work has been partially funded by the BiodivErsA and Belmont Forum project SOMBEE
594 (BiodivScen programme, ANR contract n°ANR-18-EBI4-0003-01). Alaia Morell was supported by a
595 PhD grant from Ifremer and Région Hauts-de-France. The POLCOMS-ERSEM projections were
596 produced with funding from the European Union Horizon 2020 research and innovation programme
597 under grant agreement No 678193 (CERES, Climate Change and European Aquatic Resources). The
598 authors acknowledge the Pôle de Calcul et de Données Marines (PCDM,
599 <http://www.ifremer.fr/pcdm>) for providing DATARMOR storage, data access, computational
600 resources, visualization and support services. Yunne-Jai Shin acknowledges funding support from the
601 European Union's Horizon 2020 research and innovation programme under grant agreement No
602 869300 (FutureMARES) and the Pew marine fellows programme.

603 **Conflicts of Interest**

604 The authors declare that they do not have personal interest that could have appeared to influence
605 the work reported in this paper.

606 **Author Contributions**

607 Yunne-Jai Shin and Bruno Ernande conceived and supervised the project. Bruno Ernande and Alaia
608 Morell conceived the concepts of the new model developments. Nicolas Barrier and Alaia Morell

609 developed the code and validated the model functioning. Alaia Morell gathered the data for the
610 model parameterization. Bruno Ernande and Alaia Morell conceived and developed the scripts for
611 the parameter estimation. Ghassen Halouani, Morgane Travers and Alaia Morell parameterized the
612 model. All authors interpreted the model outputs. Nicolas Barrier, Ghassen Halouani, Morgane
613 Travers and Alaia Morell performed the model calibration. Alaia Morell wrote the first paper draft. All
614 authors contributed critically to the revisions of the manuscript and gave final approval for
615 submission.

616 **Data Archiving**

617 The Bioen-OSMOSE-NS configuration and its associated version of the Bioen-OSMOSE model
618 executable will be deposited on Zenodo. Model code will be available on Github. The scripts
619 developed to estimate Bioen-OSMOSE-NS parameters are available on Github.

620 **References**

- 621 Albouy, C., Velez, L., Coll, M., Colloca, F., Le Loc'h, F., Mouillot, D., and Gravel, D. (2014). From
622 projected species distribution to food-web structure under climate change. *Global Change Biology*
623 20, 730–741. <https://doi.org/10.1111/gcb.12467>.
- 624 Amara, R., Laffargue, P., Dewarumez, J.M., Maryniak, C., Lagardère, F., and Luzac, C. (2001). Feeding
625 ecology and growth of O-group flatfish (sole, dab and plaice) on a nursery ground (Southern Bight of
626 the North Sea). *Journal of Fish Biology* 58, 788–803. [https://doi.org/10.1111/j.1095-](https://doi.org/10.1111/j.1095-8649.2001.tb00531.x)
627 8649.2001.tb00531.x.
- 628 Andersen, K.H. (2019). *Fish Ecology, Evolution, and Exploitation: A New Theoretical Synthesis*.
629 Princeton University Press.
- 630 Angilletta, M.J. (2009). *Thermal Adaptation: A Theoretical and Empirical Synthesis* (OUP Oxford).
- 631 Arcus, V.L., Prentice, E.J., Hobbs, J.K., Mulholland, A.J., Van der Kamp, M.W., Pudney, C.R., Parker,
632 E.J., and Schipper, L.A. (2016). On the Temperature Dependence of Enzyme-Catalyzed Rates.
633 *Biochemistry*, 55(12), 1681–1688. <https://doi.org/10.1021/acs.biochem.5b01094>.
- 634 Audzijonyte, A., Pethybridge, H., Porobic, J., Gorton, R., Kaplan, I., and Fulton, E.A. (2019). Atlantis: A
635 spatially explicit end-to-end marine ecosystem model with dynamically integrated physics, ecology
636 and socio-economic modules. *Methods in Ecology and Evolution* 10, 1814–1819.
637 <https://doi.org/10.1111/2041-210X.13272>.

- 638 Blanchard, J.L., Andersen, K.H., Scott, F., Hintzen, N.T., Piet, G., and Jennings, S. (2014). Evaluating
639 targets and trade-offs among fisheries and conservation objectives using a multispecies size
640 spectrum model. *Journal of Applied Ecology* 51, 612–622. <https://doi.org/10.1111/1365-2664.12238>.
- 641 Boukal, D.S., Dieckmann, U., Enberg, K., Heino, M., and Jørgensen, C. (2014). Life-history implications
642 of the allometric scaling of growth. *Journal of Theoretical Biology* 359, 199–207.
643 <https://doi.org/10.1016/j.jtbi.2014.05.022>.
- 644 Breitburg, D., Levin, L.A., Oschlies, A., Grégoire, M., Chavez, F.P., Conley, D.J., Garçon, V., Gilbert, D.,
645 Gutiérrez, D., Isensee, K., et al. (2018). Declining oxygen in the global ocean and coastal waters.
646 *Science* 359, eaam7240. <https://doi.org/10.1126/science.aam7240>.
- 647 Brosset, P., Le Bourg, B., Costalago, D., Bănar, D., Van Beveren, E., Bourdeix, J., Fromentin, J.,
648 Ménard, F., and Saraux, C. (2016). Linking small pelagic dietary shifts with ecosystem changes in the
649 Gulf of Lions. *Marine Ecology Progress Series* 554, 157–171. <https://doi.org/10.3354/meps11796>.
- 650 Brown, J.H., Gillooly, J.F., Allen, A.P., Savage, V.M., and West, G.B. (2004). TOWARD A METABOLIC
651 THEORY OF ECOLOGY. *Ecology* 85, 1771–1789. <https://doi.org/10.1890/03-9000>.
- 652 Butenschön, M., Clark, J., Aldridge, J.N., Allen, J.I., Artioli, Y., Blackford, J., Bruggeman, J., Cazenave,
653 P., Ciavatta, S., Kay, S., et al. (2016). ERSEM 15.06: a generic model for marine biogeochemistry and
654 the ecosystem dynamics of the lower trophic levels. *Geoscientific Model Development* 9, 1293–1339.
655 <https://doi.org/10.5194/gmd-9-1293-2016>.
- 656 Charnov, E.L., Turner, T.F., and Winemiller, K.O. (2001). Reproductive constraints and the evolution
657 of life histories with indeterminate growth. *Proceedings of the National Academy of Sciences* 98,
658 9460–9464. <https://doi.org/10.1073/pnas.161294498>.
- 659 Christensen, V., and Walters, C.J. (2004). Ecopath with Ecosim: methods, capabilities and limitations.
660 *Ecological Modelling* 172, 109–139. <https://doi.org/10.1016/j.ecolmodel.2003.09.003>.
- 661 Clarke, A. (2019). Energy Flow in Growth and Production. *Trends in Ecology & Evolution* 34, 502–509.
662 <https://doi.org/10.1016/j.tree.2019.02.003>.
- 663 Cohen, D.M., Inada, T., Iwamoto, T., and Scialabba, N. (1990). Gadiform fishes of the world (Order
664 Gadiformes). An annotated and illustrated catalogue of cods, hakes, grenadiers and other gadiform
665 fishes known to date. *FAO Fish. Synop.* 125(10). Rome: FAO. Vol. 10., 442 p.

- 666 Cormon, X., Kempf, A., Vermard, Y., Vinther, M., and Marchal, P. (2016). Emergence of a new
667 predator in the North Sea: evaluation of potential trophic impacts focused on hake, saithe, and
668 Norway pout. *ICES Journal of Marine Science* 73, 1370–1381.
669 <https://doi.org/10.1093/icesjms/fsw050>.
- 670 De Silva, S.S. (1973). Food and feeding habits of the herring *Clupea harengus* and the sprat *C.*
671 *sprattus* in inshore waters of the west coast of Scotland. *Marine Biology* 20, 282–290.
672 <https://doi.org/10.1007/BF00354272>.
- 673 Enberg, K., Jørgensen, C., Dunlop, E.S., Varpe, Ø., Boukal, D.S., Baulier, L., Eliassen, S., and Heino, M.
674 (2012). Fishing-induced evolution of growth: concepts, mechanisms and the empirical evidence:
675 Fishing-induced evolution of growth. *Marine Ecology* 33, 1–25. [https://doi.org/10.1111/j.1439-](https://doi.org/10.1111/j.1439-0485.2011.00460.x)
676 [0485.2011.00460.x](https://doi.org/10.1111/j.1439-0485.2011.00460.x).
- 677 Engelhard, G.H., Peck, M.A., Rindorf, A., C. Smout, S., van Deurs, M., Raab, K., Andersen, K.H., Garthe,
678 S., Lauerburg, R.A.M., Scott, F., et al. (2014). Forage fish, their fisheries, and their predators: who
679 drives whom? *ICES Journal of Marine Science* 71, 90–104. <https://doi.org/10.1093/icesjms/fst087>.
- 680 Fernandes, J.A., Cheung, W.W.L., Jennings, S., Butenschön, M., de Mora, L., Frölicher, T.L., Barange,
681 M., and Grant, A. (2013). Modelling the effects of climate change on the distribution and production
682 of marine fishes: accounting for trophic interactions in a dynamic bioclimate envelope model. *Global*
683 *Change Biology* 19, 2596–2607. <https://doi.org/10.1111/gcb.12231>.
- 684 Gillooly, James.F., Charnov, E.L., West, G.B., Savage, V.M., and Brown, J.H. (2002). Effects of size and
685 temperature on developmental time. *Nature* 417, 70–73. <https://doi.org/10.1038/417070a>.
- 686 Giraldo, C., Ernande, B., Cresson, P., Kopp, D., Cachera, M., Travers-Trolet, M., and Lefebvre, S.
687 (2017). Depth gradient in the resource use of a fish community from a semi-enclosed sea: Benthic-
688 pelagic coupling in fish diet. *Limnology and Oceanography* 62, 2213–2226.
689 <https://doi.org/10.1002/lno.10561>.
- 690 Girardin, R., Fulton, E.A., Lehuta, S., Rolland, M., Thébaud, O., Travers-Trolet, M., Vermard, Y., and
691 Marchal, P. (2018). Identification of the main processes underlying ecosystem functioning in the
692 Eastern English Channel, with a focus on flatfish species, as revealed through the application of the
693 Atlantis end-to-end model. *Estuarine, Coastal and Shelf Science* 201, 208–222.
694 <https://doi.org/10.1016/j.ecss.2016.10.016>.

- 695 Gislason, H., Daan, N., Rice, J.C., and Pope, J.G. (2010). Size, growth, temperature and the natural
696 mortality of marine fish. *Fish and Fisheries* 11, 149–158. [https://doi.org/10.1111/j.1467-](https://doi.org/10.1111/j.1467-2979.2009.00350.x)
697 2979.2009.00350.x.
- 698 Heath, M.R. (2012). Ecosystem limits to food web fluxes and fisheries yields in the North Sea
699 simulated with an end-to-end food web model. *Progress in Oceanography* 102, 42–66.
700 <https://doi.org/10.1016/j.pocean.2012.03.004>.
- 701 Heino, M., Dieckmann, U., and Godø, O.R. (2002). Measuring probabilistic reaction norms for age and
702 size at maturation. *Evolution* 56, 669–678. <https://www.jstor.org/stable/3061650>
- 703 Henriksen, O., Rindorf, A., Mosegaard, H., Payne, M.R., and van Deurs, M. (2021). Get up early:
704 Revealing behavioral responses of sandeel to ocean warming using commercial catch data. *Ecology*
705 and *Evolution*. <https://doi.org/10.1002/ece3.8310>.
- 706 Heymans, J.J., Bundy, A., Christensen, V., Coll, M., de Mutsert, K., Fulton, E.A., Piroddi, C., Shin, Y.-J.,
707 Steenbeek, J., and Travers-Trolet, M. (2020). The Ocean Decade: A True Ecosystem Modeling
708 Challenge. *Frontiers in Marine Science* 7. <https://doi.org/10.3389/fmars.2020.554573>
- 709 Holling, C.S. (1959). The Components of Predation as Revealed by a Study of Small-Mammal
710 Predation of the European Pine Sawfly¹. *The Canadian Entomologist* 91, 293–320.
711 <https://doi.org/10.4039/Ent91293-5>.
- 712 Holt, R.E., and Jorgensen, C. (2014). Climate warming causes life-history evolution in a model for
713 Atlantic cod (*Gadus morhua*). *Conservation Physiology* 2, cou050–cou050.
714 <https://doi.org/10.1093/conphys/cou050>.
- 715 ICES (2016). Report of the Benchmark Workshop on Sandeel (WKSand 2016). (31 October - 4
716 November. No. ICES CM 2016/ACOM:33).
- 717 ICES (2018a). Report of the Herring Assessment Working Group for the Area South of 62°N (HAWG)
718 (29-31 January 2018 and 12-20 March 2018).
- 719 ICES (2018b). Report of the Working Group for the Bay of Biscay and the Iberian Waters Ecoregion
720 (WGBIE) (3-10 May 2018. No. ICES CM 2018/ACOM:12).
- 721 ICES (2018c). Report of the Working Group on the Assessment of Demersal Stocks in the North Sea
722 and Skagerrak (WGNSSK) (24 April - 3 May 2018).

- 723 ICES (2019a). Catches in FAO area 27 by country, species, area and year as provided by the national
724 authorities. Source: Eurostat/ICES data compilation of catch statistics - ICES 2019, Copenhagen.
725 Version: 16-09-2019.
- 726 ICES (2019b). Working group on widely distributed stocks (WGWIDE). ICES Scientific Reports. 1:36.
727 948 pp. <http://doi.org/10.17895/ices.pub.5574>.
- 728 ICES (2021). Working Group for the Assessment of Demersal Stocks in the North Sea and Skagerrak
729 (WGNSSK) (ICES Scientific Reports).
- 730 Johnson, F.H., and Lewin, I. (1946). The growth rate of *E. coli* in relation to temperature, quinine and
731 coenzyme. *Journal of Cellular and Comparative. Physiology*, 28(1), 47–75.
732 <https://doi.org/10.1002/jcp.1030280104>.
- 733 Kooijman, S.A.L.M. (2010). *Dynamic Energy Budget Theory for Metabolic Organisation*. Cambridge
734 University Press.
- 735 Laffoley, D., and Baxter, J.M. (2019). *Ocean deoxygenation : everyone’s problem* (IUCN).
736 <https://doi.org/10.2305/IUCN.CH.2019.13.en>
- 737 Last, J.M. (1989). The food of herring, *Clupea harengus*, in the North Sea, 1983–1986. *Journal of Fish*
738 *Biology* 34, 489–501. <https://doi.org/10.1111/j.1095-8649.1989.tb03330.x>.
- 739 Lavaud, R., Thomas, Y., Pecquerie, L., Benoît, H.P., Guyondet, T., Flye-Sainte-Marie, J., and Chabot, D.
740 (2019). Modeling the impact of hypoxia on the energy budget of Atlantic cod in two populations of
741 the Gulf of Saint-Lawrence, Canada. *Journal of Sea Research* 143, 243–253.
742 <https://doi.org/10.1016/j.seares.2018.07.001>.
- 743 Law, R. (2000). Fishing, selection, and phenotypic evolution. *ICES J Mar Sci* 57, 659–668.
744 <https://doi.org/10.1006/jmsc.2000.0731>.
- 745 Lefort, S., Aumont, O., Bopp, L., Arsouze, T., Gehlen, M., and Maury, O. (2015). Spatial and body-size
746 dependent response of marine pelagic communities to projected global climate change. *Global*
747 *Change Biology* 21, 154–164. <https://doi.org/10.1111/gcb.12679>.
- 748 Lester, N.P., Shuter, B.J., and Abrams, P.A. (2004). Interpreting the von Bertalanffy model of somatic
749 growth in fishes: the cost of reproduction. *Proceedings of the Royal Society of London B: Biological*
750 *Sciences* 271, 1625–1631. <https://doi.org/10.1098/rspb.2004.2778>.

- 751 Lewy, P. (2004). A stochastic age-length-structured multispecies model applied to North Sea stocks.
752 33. <https://www.ices.dk/sites/pub/CM%20Documents/2004/FF/FF2004.pdf>
- 753 Lindmark, M., Audzijonyte, A., Blanchard, J.L., and Gårdmark, A. (2022). Temperature impacts on fish
754 physiology and resource abundance lead to faster growth but smaller fish sizes and yields under
755 warming. *Global Change Biology*. <https://doi.org/10.1111/gcb.16341>.
- 756 Mackinson, S., and Daskalov, G. (2007). An ecosystem model of the North Sea to support an
757 ecosystem approach to fisheries management: description and parameterisation.
758 <https://www.cefas.co.uk/publications/techrep/tech142.pdf>
- 759 Maury, O. (2010). An overview of APECOSM, a spatialized mass balanced “Apex Predators ECOSystem
760 Model” to study physiologically structured tuna population dynamics in their ecosystem. *Progress in
761 Oceanography* 84, 113–117. <https://doi.org/10.1016/j.pocean.2009.09.013>.
- 762 Moullec, F., Barrier, N., Guilhaumon, F., Marsaleix, P., Somot, S., and Shin, Y.-J. (2019). An End-to-End
763 model reveals losers and winners in a warming Mediterranean Sea. *Front. Mar. Sci.* 6.
764 <https://doi.org/10.3389/fmars.2019.00345>.
- 765 Ojaveer, E., and Aps, R. (2003). Sprat, *Sprattus sprattus balticus* (Schn.). p. 79-87. *Fishes of Estonia*.
766 Estonian Academy Publishers, Tallinn. 416 p.
- 767 Oliveros-Ramos, R., and Shin, Y.-J. (2016). *calibrar*: an R package for fitting complex ecological
768 models. 25. <https://doi.org/10.48550/arXiv.1603.03141>
- 769 Pawar, S., Dell, A.I., and Savage, V.M. (2015). From Metabolic Constraints on Individuals to the
770 Dynamics of Ecosystems. In *Aquatic Functional Biodiversity*, (Elsevier), pp. 3–36.
771 <https://doi.org/10.1016/B978-0-12-417015-5.00001-3>
- 772 Piet, G.J., Pfisterer, A.B., and Rijnsdorp, A.D. (1998). On factors structuring the flatfish assemblage in
773 the southern North Sea. *Journal of Sea Research* 40, 143–152. [https://doi.org/10.1016/S1385-
774 1101\(98\)00008-2](https://doi.org/10.1016/S1385-1101(98)00008-2).
- 775 Pikitch, E.K., Santora, C., Babcock, E.A., Bakun, A., Bonfil, R., Conover, D.O., Dayton, P., Doukakis, P.,
776 Fluharty, D., Heneman, B., et al. (2004). Ecosystem-Based Fishery Management. *Science* 305, 346–
777 347. <https://doi.org/10.1126/science.1098222>.

- 778 Pörtner, H.O. (2001). Climate change and temperature-dependent biogeography: oxygen limitation
779 of thermal tolerance in animals. *Naturwissenschaften* 88, 137–146.
780 <https://doi.org/10.1007/s001140100216>
- 781 Quince, C., Abrams, P.A., Shuter, B.J., and Lester, N.P. (2008). Biphasic growth in fish I: Theoretical
782 foundations. *Journal of Theoretical Biology* 254, 197–206. <https://doi.org/10.1016/j.jtbi.2008.05.029>.
- 783 Raab, K., Nagelkerke, L. a. J., Boerée, C., Rijnsdorp, A.D., Temming, A., and Dickey-Collas, M. (2012).
784 Dietary overlap between the potential competitors herring, sprat and anchovy in the North Sea.
785 *Marine Ecology Progress Series* 470, 101–111. <https://doi.org/10.3354/meps09919>.
- 786 Rijnsdorp, A.D., and Vingerhoed, B. (2001). Feeding of plaice *Pleuronectes platessa* L. and sole *Solea*
787 *solea* (L.) in relation to the effects of bottom trawling. *Journal of Sea Research* 45, 219–229.
788 [https://doi.org/10.1016/S1385-1101\(01\)00047-8](https://doi.org/10.1016/S1385-1101(01)00047-8).
- 789 Robb, A.P., and Hislop, J.R.G. (1980). The food of five gadoid species during the pelagic O-group
790 phase in the northern North Sea. *Journal of Fish Biology* 16, 199–217.
791 <https://doi.org/10.1111/j.1095-8649.1980.tb03699.x>.
- 792 Rose, K.A., Allen, J.I., Artioli, Y., Barange, M., Blackford, J., Carlotti, F., Cropp, R., Daewel, U., Edwards,
793 K., Flynn, K., et al. (2010). End-To-End Models for the Analysis of Marine Ecosystems: Challenges,
794 Issues, and Next Steps. *Marine and Coastal Fisheries* 2, 115–130. <https://doi.org/10.1577/C09-059.1>.
- 795 Serpetti, N., Baudron, A.R., Burrows, M.T., Payne, B.L., Helaouët, P., Fernandes, P.G., and Heymans,
796 J.J. (2017). Impact of ocean warming on sustainable fisheries management informs the Ecosystem
797 Approach to Fisheries. *Sci Rep* 7, 13438. <https://doi.org/10.1038/s41598-017-13220-7>.
- 798 Shin, Y.-J., and Cury, P. (2004). Using an individual-based model of fish assemblages to study the
799 response of size spectra to changes in fishing. *Canadian Journal of Fisheries and Aquatic Sciences* 61,
800 414–431. <https://doi.org/10.1139/f03-154>.
- 801 Stäbler, M., Kempf, A., Mackinson, S., Poos, J.J., Garcia, C., and Temming, A. (2016). Combining
802 efforts to make maximum sustainable yields and good environmental status match in a food-web
803 model of the southern North Sea. *Ecological Modelling* 331, 17–30.
804 <https://doi.org/10.1016/j.ecolmodel.2016.01.020>.
- 805 Stearns, S.C. (1992). *The Evolution of Life Histories* (OUP Oxford).

- 806 Stearns, S.C., and Koella, J.C. (1986). The Evolution of Phenotypic Plasticity in Life-History Traits:
807 Predictions of Reaction Norms for Age and Size at Maturity. *Evolution* 40, 893–913.
808 <https://doi.org/10.2307/2408752>.
- 809 Steenbeek, J., Buszowski, J., Chagaris, D., Christensen, V., Coll, M., Fulton, E.A., Katsanevakis, S.,
810 Lewis, K.A., Mazaris, A.D., Macias, D., et al. (2021). Making spatial-temporal marine ecosystem
811 modelling better – A perspective. *Environmental Modelling & Software* 145, 105209.
812 <https://doi.org/10.1016/j.envsoft.2021.105209>.
- 813 Teal, L.R., Hal, R. van, Kooten, T. van, Ruardij, P., and Rijnsdorp, A.D. (2012). Bio-energetics underpins
814 the spatial response of North Sea plaice (*Pleuronectes platessa* L.) and sole (*Solea solea* L.) to climate
815 change. *Global Change Biology* 18, 3291–3305. <https://doi.org/10.1111/j.1365-2486.2012.02795.x>.
- 816 Thomas, Y., Flye-Sainte-Marie, J., Chabot, D., Aguirre-Velarde, A., Marques, G.M., and Pecquerie, L.
817 (2019). Effects of hypoxia on metabolic functions in marine organisms: Observed patterns and
818 modelling assumptions within the context of Dynamic Energy Budget (DEB) theory. *Journal of Sea
819 Research* 143, 231–242. <https://doi.org/10.1016/j.seares.2018.05.001>.
- 820 Timmerman, C.-A., Marchal, P., Denamiel, M., Couvreur, C., and Cresson, P. (2020). Seasonal and
821 ontogenetic variation of whiting diet in the Eastern English Channel and the Southern North Sea.
822 *PLOS ONE* 15, e0239436. <https://doi.org/10.1371/journal.pone.0239436>.
- 823 Timmerman, C.-A., Giraldo, C., Cresson, P., Ernande, B., Travers-Trolet, M., Rouquette, M., Denamiel,
824 M., and Lefebvre, S. (2021). Plasticity of trophic interactions in fish assemblages results in temporal
825 stability of benthic-pelagic couplings. *Marine Environmental Research* 170, 105412.
826 <https://doi.org/10.1016/j.marenvres.2021.105412>.
- 827 Travers, M., Shin, Y.-J., Jennings, S., and Cury, P. (2007). Towards end-to-end models for investigating
828 the effects of climate and fishing in marine ecosystems. *Progress in Oceanography* 75, 751–770.
829 <https://doi.org/10.1016/j.pocean.2007.08.001>.
- 830 Travers, M., Shin, Y.-J., Jennings, S., Machu, E., Huggett, J.A., Field, J.G., and Cury, P.M. (2009). Two-
831 way coupling versus one-way forcing of plankton and fish models to predict ecosystem changes in
832 the Benguela. *Ecological Modelling* 220, 3089–3099.
833 <https://doi.org/10.1016/j.ecolmodel.2009.08.016>.
- 834 Travers-Trolet, M., Coppin, F., Cresson, P., Cugier, P., Oliveros-Ramos, R., and Verley, P. (2019).
835 Emergence of negative trophic level-size relationships from a size-based, individual-based

- 836 multispecies fish model. *Ecological Modelling* 410, 108800.
837 <https://doi.org/10.1016/j.ecolmodel.2019.108800>.
- 838 Urban, M.C., Bocedi, G., Hendry, A.P., Mihoub, J.-B., Pe'er, G., Singer, A., Bridle, J.R., Crozier, L.G., De
839 Meester, L., Godsoe, W., et al. (2016). Improving the forecast for biodiversity under climate change.
840 *Science* 353, aad8466. <https://doi.org/10.1126/science.aad8466>.
- 841 Vaquer-Sunyer, R., and Duarte, C.M. (2008). Thresholds of hypoxia for marine biodiversity.
842 *Proceedings of the National Academy of Sciences* 105, 15452–15457.
843 <https://doi.org/10.1073/pnas.0803833105>.
- 844 van Wijk, S.J., Taylor, M.I., Creer, S., Dreyer, C., Rodrigues, F.M., Ramnarine, I.W., van Oosterhout, C.,
845 and Carvalho, G.R. (2013). Experimental harvesting of fish populations drives genetically based shifts
846 in body size and maturation. *Frontiers in Ecology and the Environment* 11, 181–187.
847 <https://doi.org/10.1890/120229>.